CROSS SECTIONS FOR NEUTRON PRODUCTION AT ZERO DEGREES BY THE $^{3}H(p,n)$ REACTION.

BY

PHILIP MOHAN THAMBIDURAI

A THESIS SUBMITTED TO THE GRADUATE FACULTY OF
NORTH CAROLINA STATE UNIVERSITY
IN PARTIAL FULFILLMENT OF THE
REQUIREMENT FOR THE DEGREE OF
MASTER OF SCIENCE.

DEPARTMENT OF PHYSICS

RALEIGH,N.C.

APPROVED BY

_____ _____

_____

CHAIRMAN OF ADVISORY COMMITTEE.

ABSTRACT

THAMBIDURAI, PHILIP MOHAN. Cross-sections for neutron production at zero degrees by the $^{3}H(p,n)$ reaction.(Under the direction of Dr.CHRISTOPHER GOULD).

Pulsed proton beams of energies 8.27, 9.77, 10.77, 11.77, 12.77, 13.77 and 14.77 MeV were produced at the Triangle Universities Nuclear Laboratory's FN Tandem Van de Graaff accelerator. These were incident on a gaseous tritium target. Neutrons produced by $^{3}H(p,n)$ reactions were detected at zero degrees in a well shielded NE-218 liquid scintillator at the flight path of 2.785 meters. Neutron energy spectra were obtained by measuring the time of flight of the neutrons. The data were converted to zero-degree double differential cross-sections (mb/sr.MeV) for neutron emission. Total zero-degree break-up cross-sections were obtained at each incident proton energy by summing over double differential cross-sections. Pure 3-body phase-space fits are made to the observed continuum neutron cross-sections.

BIOGRAPHY

PHILIP MOHAN THAMBIDURAI

Born: 7 October 1956, Munnar,Kerala State,India

Education: High School,St.Johns Vestry School, Tiruchirappalli,India.

Pre-University,St.Joseph's College, Tiruchirappalli,India.(1974)

B.S. Physics and Chemistry, Geneva College, Beaver Falls, Pennsylvania.(1978)

ACKNOWLEDGEMENTS

I wish to express my deepest gratitude to Dr.Chris Gould for the guidance, direction and encouragement that he has provided to me throughout the course of my career at NCSU. Also I owe very much to Al Beyerle for his patient help in many things. The experiment was made possible by the cooperation and effort of several people at TUNL, most of all Dr.L.W.Seagondollar. The U.S.Department of Energy was responsible for part of the funding for this project.

And I am indebted to my parents for their support (all kinds) during my entire career .

TABLE OF CONTENTS

INTRODUCTION

The $^{3}H(p,n)^{3}He$ reaction is a common source of mono-energetic neutrons in nuclear physics experiments. These neutrons are then used in elastic and inelastic scattering measurements which study the nuclear potential and the structure of the nucleus. The neutron is especially convenient as a projectile because it does not interact with the Coulomb field of the nucleus. Neutrons having energies up to several hundred MeV can be produced. In the $^{3}H(p,n)^{3}He$ reaction, the neutrons have an energy at zero degrees which is approximately 770 keV below that of the incident proton beam. As the incident proton energy is increased it is found that there is not just a single mono-energetic group of neutrons (corresponding to the ^{3}He ground state); what is seen in addition is a continuum of lower energy outgoing neutrons. These lower energy neutrons result from 3 and 4-body processes in which the ^{3}He nucleus breaks up into p+d or p+p+n. Breakup of the p + ^{3}He system into three bodies (n+p+d) becomes energetically possible when the proton energy is greater than 8.34 MeV; four-body break-up (p+p+n+n) is allowed for a proton energy greater than 11.3 MeV. We call these lower energy neutrons 'break-up' neutrons in what follows. There is no suitable way of selectively suppressing these low energy neutrons in an experiment where the primary neutron group has an energy

above 7.5 MeV. We have to measure the cross section for their production and later account for their effects when describing the data of interest.

There are two other reactions involving hydrogen gas targets which are also suitable for neutron production. In the $^{2}H(d,n)^{3}He$ reaction the yield of mono-energetic neutrons at zero degrees is about a factor of 2.5 greater compared to the $^{3}H(p,n)^{3}He$ reaction. In the $^{1}H(t,n)^{3}He$ reaction in which a triton beam bombards a hydrogen gas target, the yield is almost 20 times more than the $^{3}H(p,n)^{3}He$ reaction. However, the break-up cross section in the $^{2}H(d,n)^{3}He$ reaction is a factor of 10 larger than for the $^{3}H(p,n)^{3}He$ reaction, so that one prefers the latter if a minimum amount of background is desirable. The $^{1}H(t,n)^{3}He$ reaction is usually the least desirable due to the problem of tritium contamination and the difficulties associated with obtaining a triton beam. The best data available (till 1973) from the above three reactions (information on break-up cross sections was not included) for proton energies up to 10.0 MeV was given by Liskien and Paulsen.[1] More recently the break-up cross sections for the three reactions have been measured at zero degrees by Drosg et al[2,3] at LASL. Until now these were the only data existing for the measurement of the break-up cross sections for tritium break-ups. The measurements at TUNL were undertaken to verify the results of Drosg et al and to obtain a better determination of the shape of the continuum neutron spectra at zero degrees.

At TUNL there has been a program of neutron scattering experiments on medium and heavy-mass nuclei to obtain a compilation of neutron cross sections. These elements are being studied for the possibility of their use in the construction of the fusion reactor, where the fast-neutron flux is extremely high. Neutrons produced by the fusion of tritium and deuterium have an initial energy of just over 14 MeV. Due to the scattering of these neutrons, a spectrum of neutrons is expected peaking around 14 MeV. This energy region can be duplicated at TUNL. The $^{3}H(p,n)^{3}He$ reaction has been employed as a neutron source at TUNL. For this we require an accurate measurement of the associated backgrounds (i.e. the break-ups). As part of this program, the $^{3}H(p,n)X,Y$ cross sections were measured in this experiment, for proton energies ranging from 9.77 MeV to 14.77 MeV.

I

DESCRIPTION OF THE EXPERIMENT

The facilities available at the Triangle Universities Nuclear Laboratory were utilized to study the neutron spectrum produced by the $^{3}H(p,n)$ reaction. A general layout of the experimental area is depicted in figure 1.1 . The FN Tandem Van de Graaff has a maximum terminal voltage of 8 million volts and is capable of producing proton beams of energy up to 16 MeV. The energy resolution of the final proton beam is about 100 keV. A direct-extraction negative ion source provided the initial H^{-} beam of energy 50 keV for injection into the accelerator. Prior to acceleration the beam was pulsed at a rate f=2 MHz. A buncher was then used to obtain a frequency of either f/16 or f/32 for this experiment. Beam-line vacuum was maintained at about 10^{-6} torr by several diffusion pumps using liquid-nitrogen trapping , and also by a turbo-molecular pump.

TRITIUM CELL AND FILLING SYSTEM

The fast neutrons were produced by having the protons bombard gaseous tritium contained in a cylindrical cell (figure 1.2) of volume 0.5 cm^{3} at the end of the beam line.

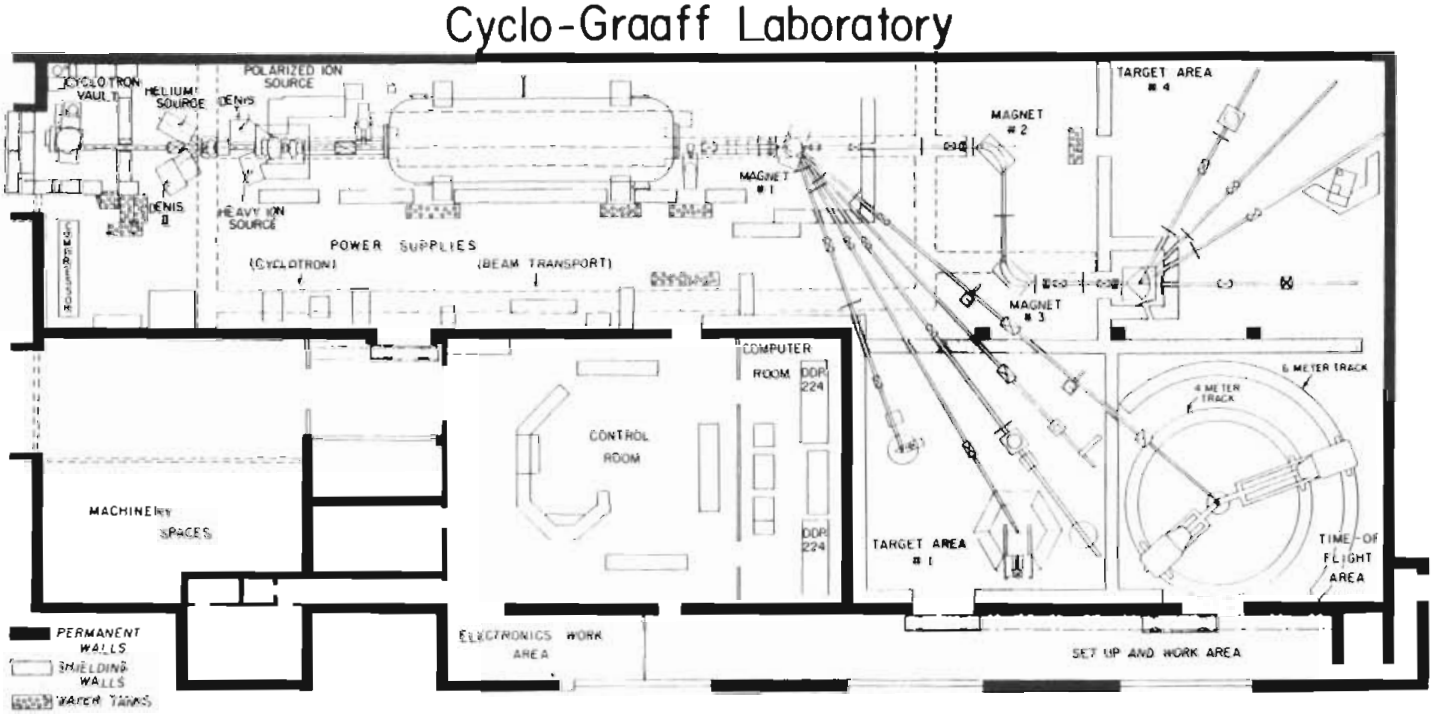

Figure 1.1 Layout of the tandem facility at TUNL.

The cell itself was made of tantalum. The entrance foil and the beam stop (6 mg/cm^2) were made of ^{58}Ni in order to minimize neutron production from (p,n) reactions.[2] The tritium had been adsorbed into uranium pellets contained in a metal tube (the uranium 'furnace', see figure 1.3). When required, the gas was expelled into the gas-cell by heating this furnace. At a temperature of about 400 degrees celsius the gas begins to escape. After continuous heating at 600 degrees for a few minutes, most of the tritium comes out. Valve 3 is then closed (figure 1.3). To pump the gas back the valve is opened up thus enabling the tritium to be adsorbed back into the furnace. A comparison of predicted versus observed cross sections showed that the purity of the tritium in the cell for the initial filling was about 90%, decreasing to less than 85% for subsequent fillings.

Gas pressure was monitored by a standard pressure gauge and by a silicon pressure transducer manufactured by National Semiconductor (model LX-1704GB). The transducer was the 'backward-gauge' type ----i.e. the gas does not directly come into contact with the actual solid state sensor, but is separated by a very thin membrane. This reduces the chances of a leak and also protects the transducer from corrosive gases . This transducer needed an active volume of only 0.5 cm^3 . This is an important factor to be considered in the selection of a gauge because the amount of tritium available in the furnace is limited, and

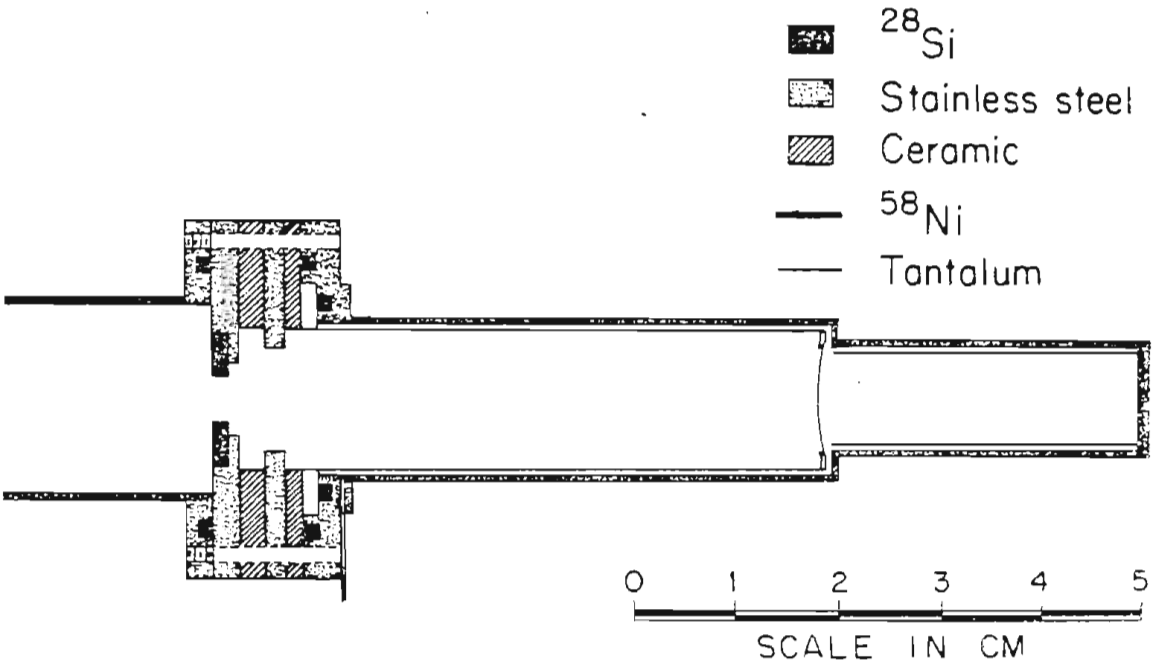

Figure 1.2 Cross-section of the tritium gas cell.[10]

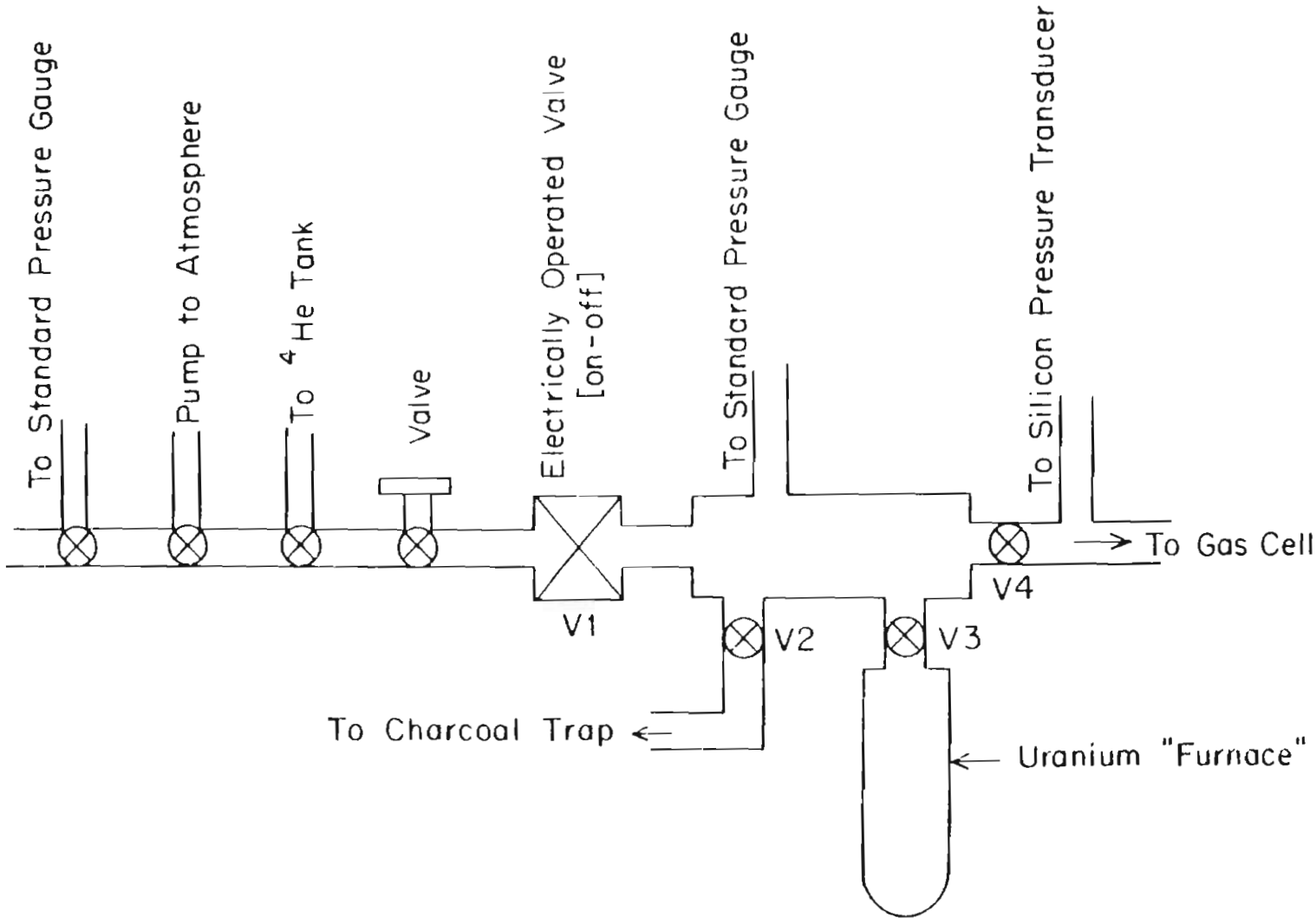

Figure 1.3 Tritium filling system.

it is therefore necessary to minimize the volume of the gas-transport system. Also, in the event that the foil ruptures, the tritium contamination of the beam pipe should be minimal. The transducer provides an output signal which is directly proportional to the pressure. This signal was scaled such that a digital readout in absolute pounds per square inch was available at the gas-filling area and also at the control room (figure 1.4). The signal was also connected to a d'Arsonval meter which could trigger an alarm system. An additional output was connected to a chart recorder to monitor pressure changes over long periods of time. It was found that the linearity of the transducer far exceeded the specified range. At least during the course of this experiment, the performance[4] of the transducer was not affected by the intense gamma and neutron radiation present in that area.

The entire filling system was under a hood through which the air in the room was constantly being evacuated. The target room itself was kept a little below atmospheric pressure, as a safety precaution. A fast-acting locomotive valve ensured that the accelerator tube would not be contaminated in the event of a tritium leak. The gas-cell is cooled by an air jet.

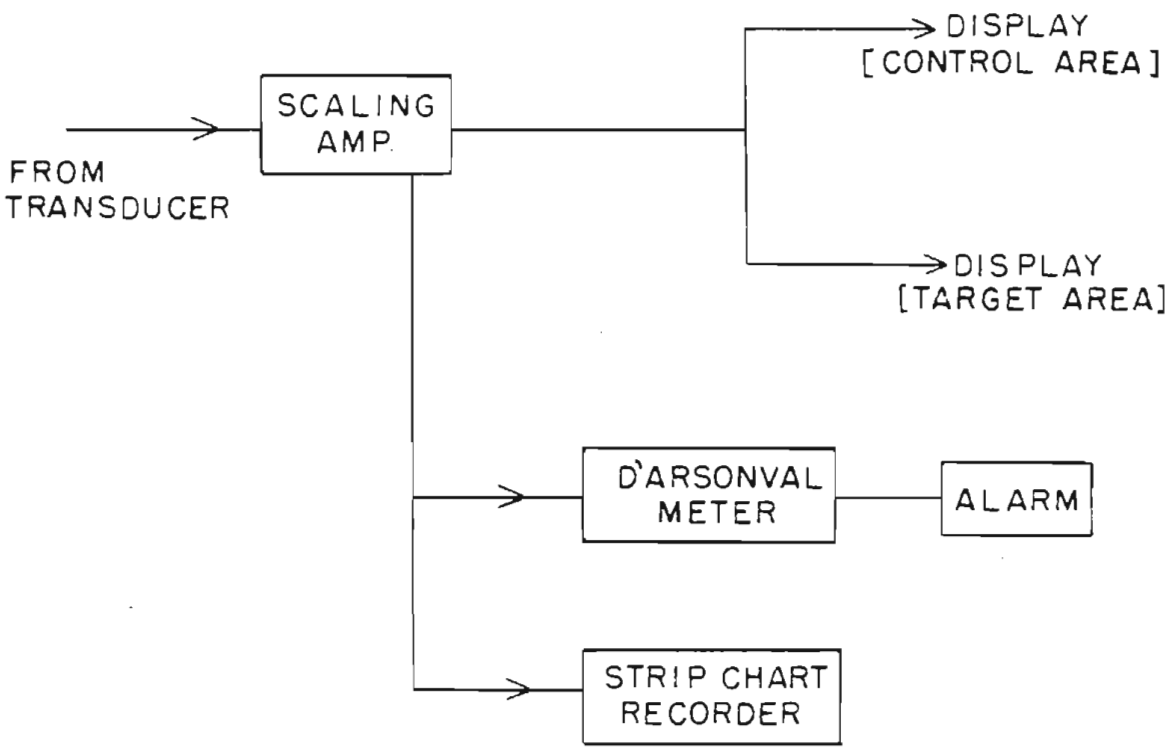

Figure 1.4 Tritium monitor system.

NEUTRON DETECTION

The neutrons were detected in a NE-218 liquid scintillator at zero degrees and at a distance of 2.785 meters from the tritium target. The detector (dimensions: 6.35 cm. thick , 8.89 cm. diameter) is very well shielded and is mounted on wheels moving in a circular track. The 5-ton shield consists mostly of a mixture of paraffin and lithium carbonate encased in copper and lead (figure 1.5). Flight paths from 2.5 meters to 3.9 meters are possible.

Such detectors have different efficiencies for different neutron energies because the H(n,p) cross-section varies with energy. Therefore it is necessary to know this efficiency from previous calibration measurements. A plot of the efficiency of this system is in figure 1.6 . The curved line is a fit to the actual data points. The low-energy bias was set just where the efficiency drops rapidly (about 300 keV). A point between the 60 keV gamma peak of ^{247}Am and its Compton edge was chosen as the bias point.

ELECTRONICS

The flight times of the neutrons were measured by the electronics shown schematically in figure 1.7 . The fast negative-going linear signal from the anode of the

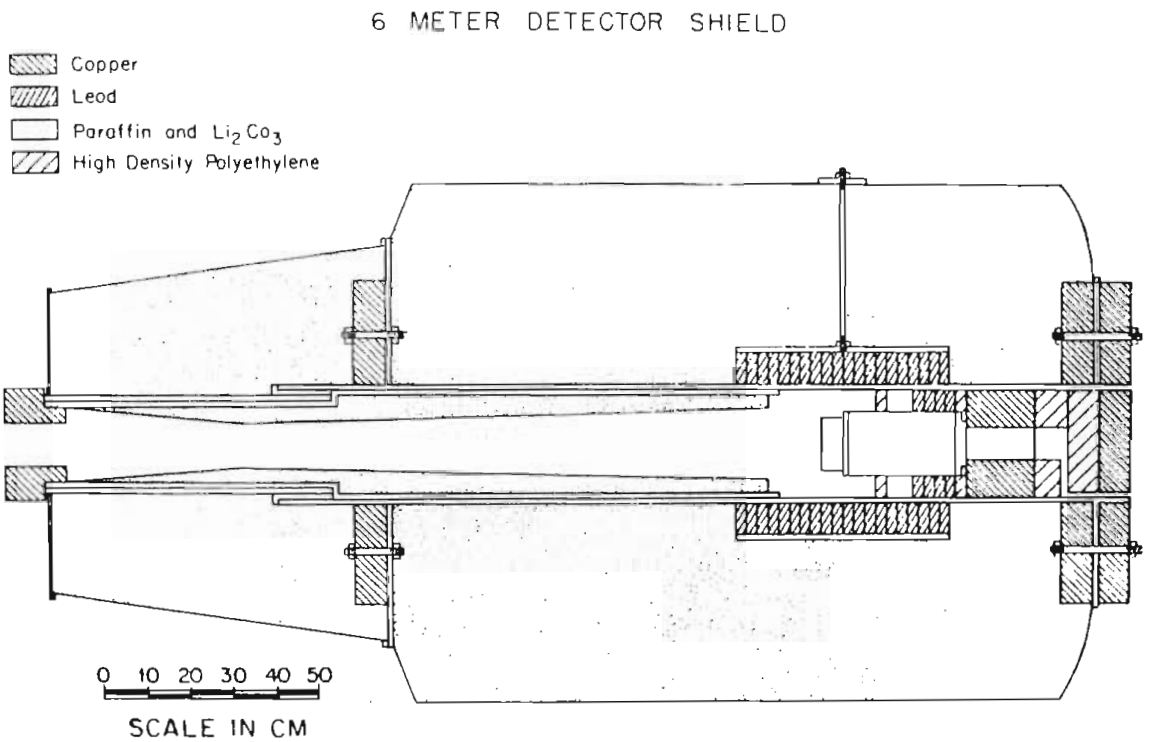

Figure 1.5 Cross-section of the detector and shielding.[11]

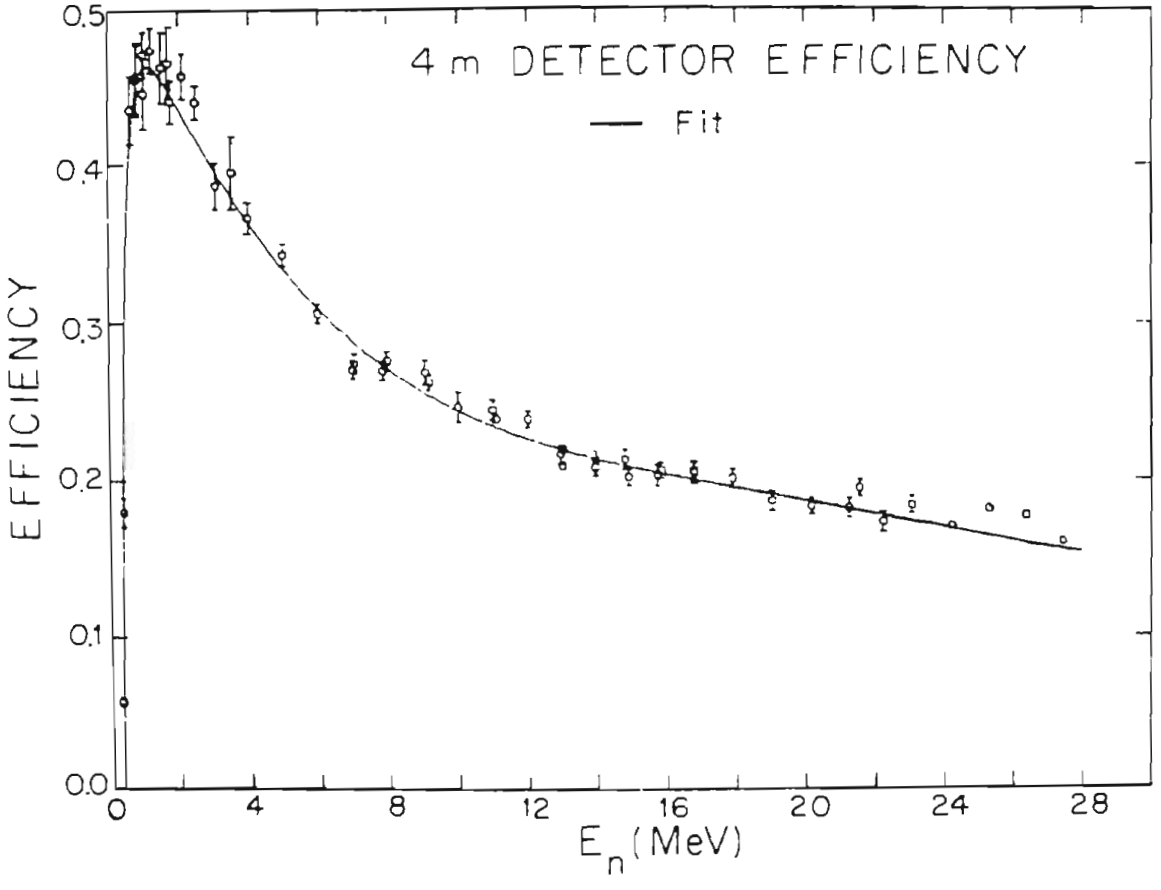

Figure 1.6 Detector efficiency; the curve is a best-fit to the data points.[12]

photomultiplier tube is routed to three different units ---- a Pulse Shape Discriminator (PSD), a Constant Fraction Discriminator (CFD) and a fast amplifier with a Single Channel Analyzer (SCA). The CFD provides a fast logic signal for every input pulse . This occurs just when the input crosses a certain level during its rise to the peak value, the level itself being at a constant fraction of the peak ; this level can be set. Thus the CFD triggers at a very precise time, so the output is chosen as one point of reference for the timing information. This becomes the 'start' signal for a Time-to-Amplitude Converter (TAC) , which is a device that will put out a signal whose amplitude is directly proportional to the time interval between two input pulses ('start' and 'stop'). The stop signal to the TAC comes from a capacitive 'pick-off' near the end of the beam-pipe. The output (I) of the TAC is now proportional to the time of flight of the detected particle.

The anode signal is also the input signal to the PSD. The PSD is capable of differentiating between signals that are due to neutrons and those that are due to gamma radiation. This arises from the fact that the neutron and gamma interact by different means with the liquid scintillator, resulting in signals with different rise times. Inside the PSD the anode pulse is integrated and differentiated (S1 in figure 1.8), which results in the zero-crossing points of the neutron and gamma pulses being

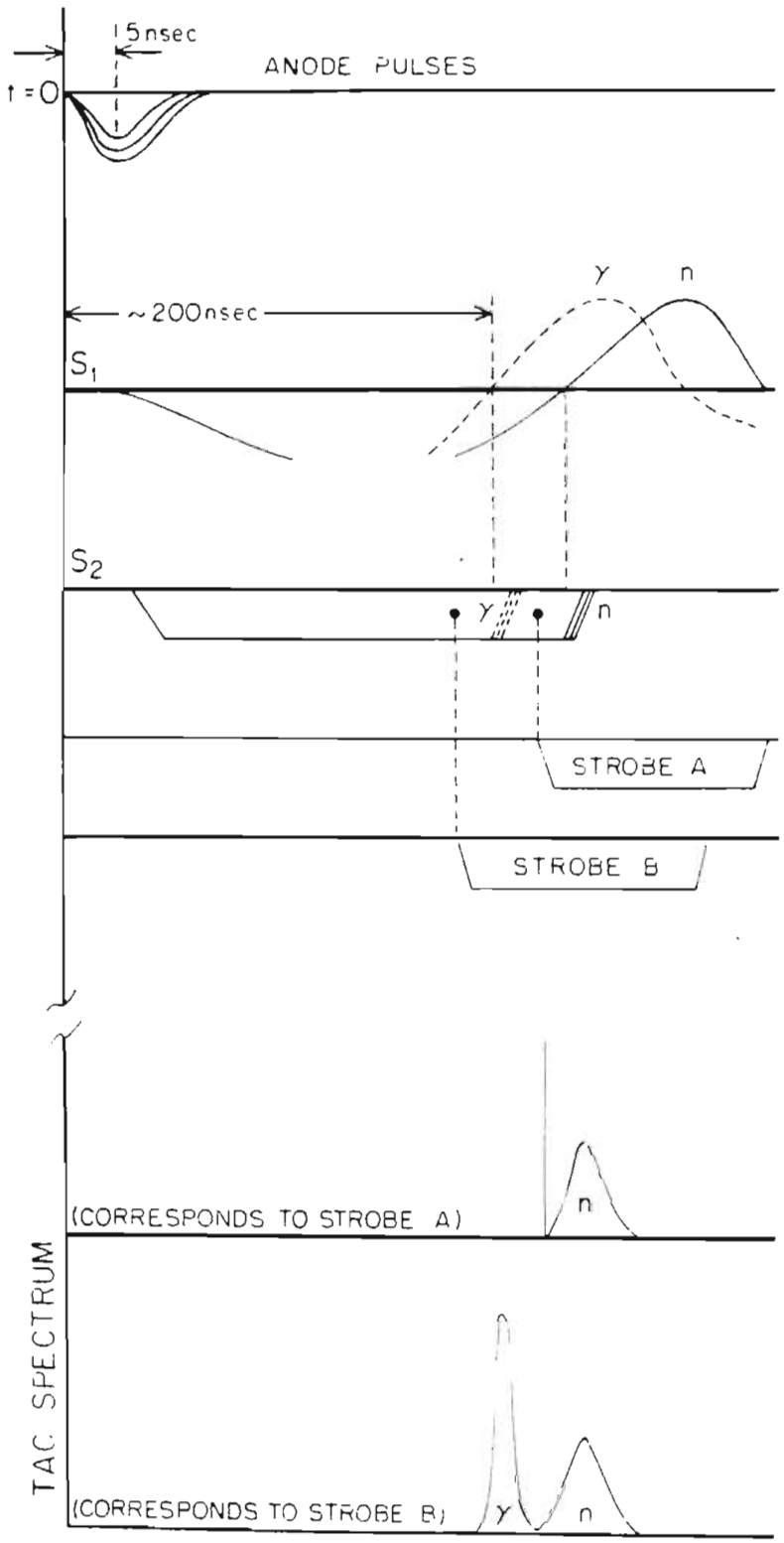

Figure 1.8 Pulse-shape-discrimination.

different. This is enhanced by another internal amplifier within the PSD (S2 in figure 1.8). The strobe input to the PSD can be delayed such that it comes in as shown in figure 1.8 (strobe A); in which case only the neutron signals will be passed out of the unit. This becomes the 'stop' input to a TAC which is started by the constant fraction discriminator. The output of the TAC as seen on a multi-channel-analyzer is also shown in figure 1.8 . Only the neutron spectrum is seen. The PSD may also be strobed so that both neutron and gamma signals are passed. By using strobe B in figure 1.8 the corresponding TAC spectrum shows a clear distinction between neutron and gamma. In the experiment the PSD was operated in the neutron+gamma mode. This TAC also has a single channel analyzer whose window is set to pass only the neutrons. Its output goes to the 'gate' input of a 'Linear Gate and Stretcher' via a coincidence unit. Another input to this coincidence is the delayed positive output from the PSD. Now this signal remains 'ON' when a neutron or gamma pulse is present, and it is dependent on the output of the CFD, since the strobe input for the PSD comes from the CFD. Therefore this was used to set the low-energy bias. The linear input to the Linear Gate & Stretcher is the neutron time of flight signal. It is digitized in an analog to digital converter and stored in a Honeywell DDP-224 computer. The computer program allows for several operations to be performed on the

data, which are displayed in real time. The data were transferred regularly to magnetic tape for later analysis.

II

EXPERIMENTAL PROCEDURE AND DATA ANALYSIS

Data were taken for incident proton energies 8.27,9.77,10.77,11.77,12.77,13.77 and 14.77 MeV. The threshold for the production of break-up neutrons via the $^{3}H(p,n)$ reaction is 8.34 MeV. Table 2.1 lists the thresholds and Q-values for the different break-up channels; table 2.2 shows the maximum energy that the neutron can have at zero degrees if produced by the $^{3}H(p,n)d,p$ channel. All throughout the experiment the proton beam was stable, the current at the target being typically 40-50 nano-amperes. At each energy data were accumulated for about one hour. Gas pressure was 1.5 atmospheres and this did not change significantly during data acquisition.

Figure 2.1 is the raw neutron time-of-flight spectrum obtained with tritium in the cell for protons of energy 12.77 MeV. The tall peak at a flight time of about 50 nsec. arises from the $^{3}H(p,n)^{3}He$ reaction. The peaks further to the right are gamma rays which were not eliminated by the neutron-gamma discrimination. In order to eliminate all backgrounds, data were also taken with ^{4}He in the cell for a similar time and pressure as the tritium data. In the

helium spectrum (figure 2.2) we can see the same broad structure as the tritium; now the ^{3}He peak is not present. On closer inspection it is clear that the sharp structures on the broad continuum of both spectra match exactly. The effect of the subtraction (^{3}H-^{4}He) can be seen clearly in figure 2.3 . Now the broad continuum has lost its structure and the gamma peaks present before have also disappeared. The contribution from (p,n) processes in the materials of the gas cell and from collisions with the slits and beam-pipe are removed by this subtraction. In figure 2.3 the broad hump represents neutrons coming from break-up processes while the tall peak is the ^{3}He peak, which is normally used as a mono-energetic neutron source.

A horizontal background was drawn and subtracted near the baseline of the time-of-flight spectrum; this background was extremely small. Then the time scale was transformed to an energy scale, taking into account the dead-time and the efficiency of the scintillator. The count in each channel was normalized to the number of protons incident on the target as determined by beam current integration. Figure 2.4 shows such a spectrum for E_p =12.77 MeV. The broad continuum at lower energies is due to the break-up of the 3 and 4-body systems and the tall peak is the ^{3}He ground state.

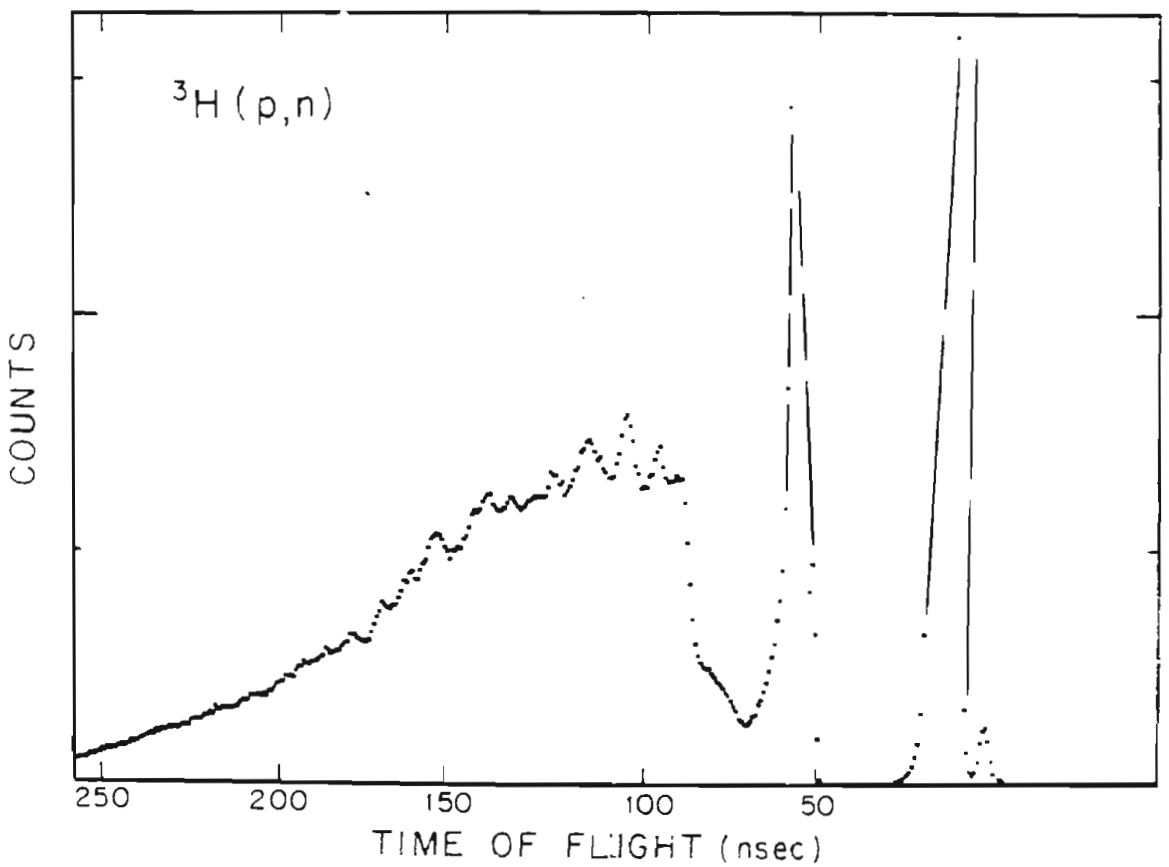

Figure 2.1 Neutron time of flight spectrum with the tritium target.

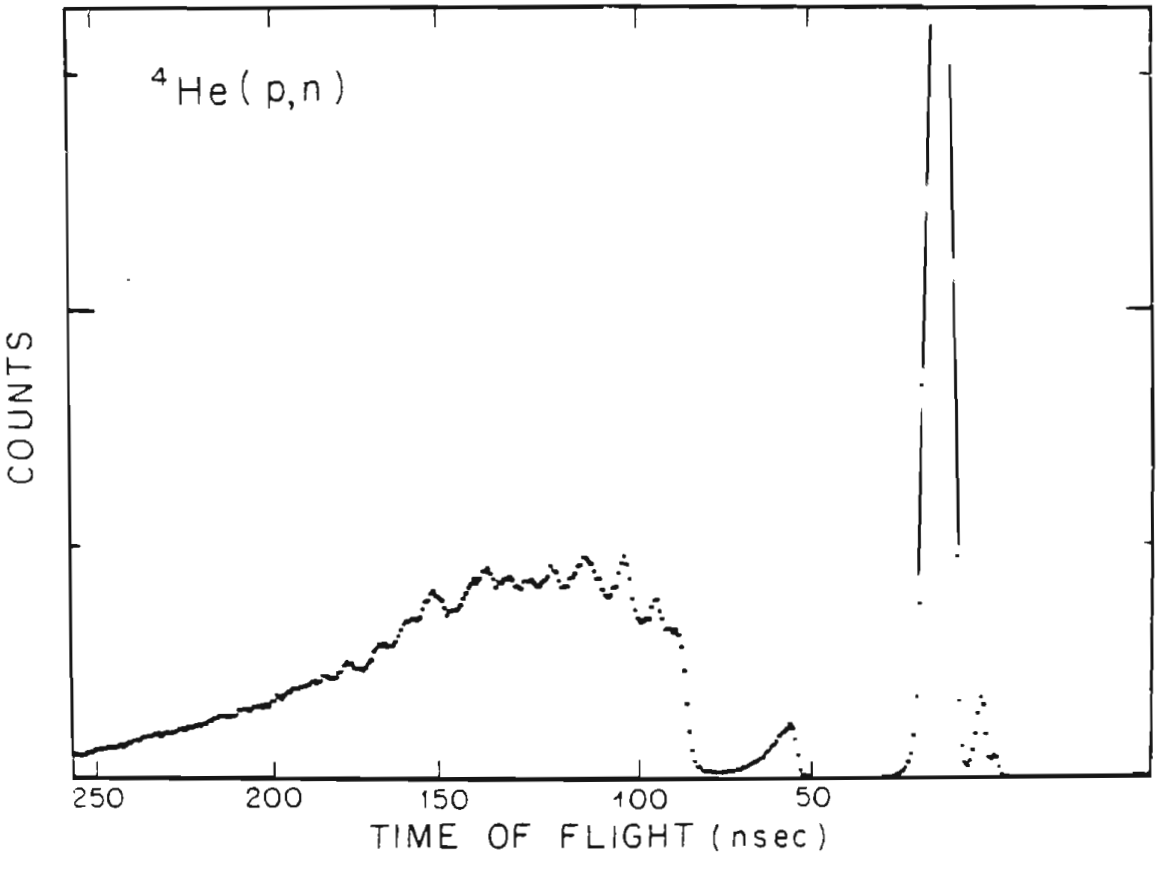

Figure 2.2 Neutron time of flight spectrum with the helium target.

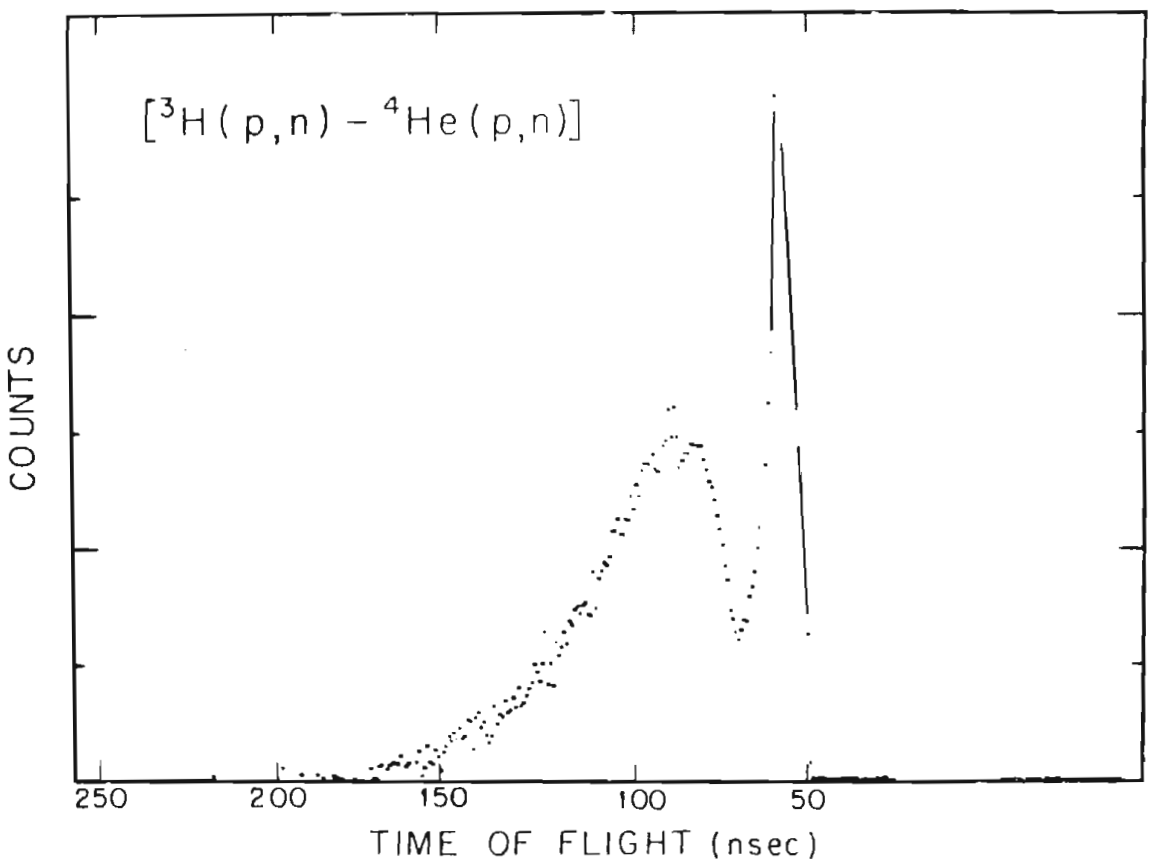

Figure 2.3 Neutron time of flight spectrum after the subtraction.

Up to this point the analysis was done on a Honeywell DDP-224 computer. All further analysis was done in the Digital Equipment Corporation VAX/VMS 11/780 system.

Table 2.1

Q-values and thresholds.

Reaction	Q-value (MeV)	Threshold (MeV)
$^{3}H(p,n)^{3}He$	-0.764	1.02
$^{3}H(p,n)d,p$	-6.26	8.34
$^{3}H(p,2n)2p$	-8.34	11.3

Table 2.2

Maximum energy of the neutron emitted at zero degrees in the laboratory frame for the reaction $^{3}H(p,n)d,p$.

Incident Proton energy (MeV)	Neutron energy (MeV)
9.77	2.81
10.77	3.96
11.77	5.05
12.77	6.11
13.77	7.16
14.77	8.20

Table 2.3

Ratio of background type 2 to the total area in the continuum.

Proton energy (MeV)	Area of background ÷ Total area
9.77	0.45
10.77	0.31
11.77	0.22
12.77	0.24
13.77	0.22
14.77	0.24

Table 2.4

Yields in the ^{3}He ground state peak.

E_n	Filling #	Experimental ÷ calculated	Corrected ratio
7.5	1	0.80	
13.0	1	0.64	0.67
12.0	2	0.68	0.71
11.0	3	0.76	0.78
10.0	3	0.80	0.82
14.0	4	0.58	0.62

The count per energy bin was then converted to a cross-section in millibarns per steradian per MeV by normalising it to the known cross-section for the ^{3}He ground state peak. Data of ref.2 were used for this purpose. Now we have the 'double differential cross-sections' for neutron production at zero degrees. This may be interpreted as the probability for the neutron to be observed at zero degrees and having a particular energy. Usually this quantity is denoted by $\frac{d^2\sigma}{d\Omega\, dE}$.

In a plot of the cross-section vs. energy (figure 2.4) one can see two main features, the break-up continuum and the ^{3}He g.s.peak. The break-up process can produce neutrons having energies below a certain maximum energy which is determined solely by the kinematics (table 2.2). The primary neutron peak (^{3}He g.s.) should occur exactly at an energy determined by the incident proton energy. Between these two energies then, we do not expect any neutrons---at least none that are produced by the T+p reaction. The finite resolution of the detector is primarily responsible for the small spread of energies in the ground state peak. The data (figures 2.5 - 2.7)show that there are neutrons in this intermediate region. On closer examination there seems to be a gradually dropping 'tail' from the primary peak, to its left. It is reasonable to assume that this tail still

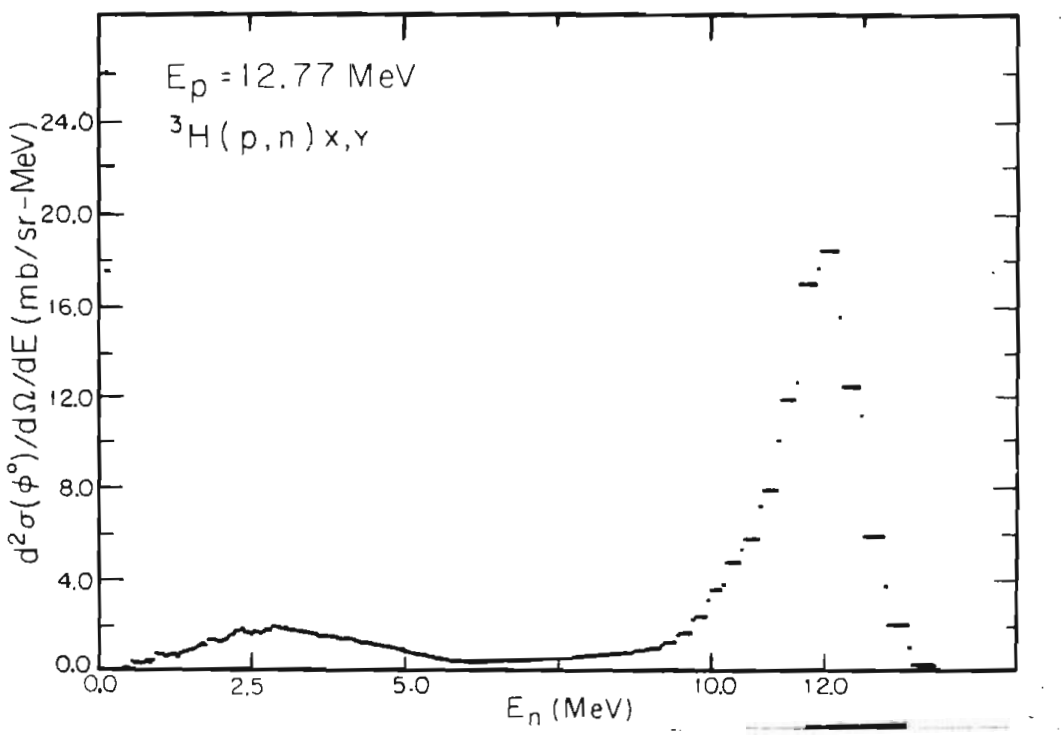

Figure 2.4 Raw data after transforming the time scale to an energy scale.

exists at lower energies (under the break-up region) and goes to zero at zero neutron energy. We need to know the shape of this tail in order to calculate the break-up cross-section. One can at best make an estimate of the background. A flat background (figure 2.7) should remove all the contribution from the tail; this is surely an upper limit and also unreasonable because the tail is definitely there. Type 3 in the same figure may be taken as a minimum case where the tail decreases to zero quite rapidly,in a linear manner. A middle course (type 2) was adopted as the most reasonable. While doing this, the uncertainties reported include the possibility that one of the other two kinds of background may be more correct. We can understand better the nature of this tail by looking at data which were taken below the threshold for production of break-up neutrons (figure 2.9). The tail is still very much present and its shape justifies the type of background used for the above-threshold data. The sharp peaks in the data will be discussed later. In table 2.3 the ratio of the counts in this tail (type 2) to the total counts in the continuum (without subtraction) are given. The numbers show that the tailing effect cannot be neglected. The area of this tail extends from 45% of the total break-up cross-section at E_p = 9.77 MeV to 22% at E_p = 13.77 MeV.

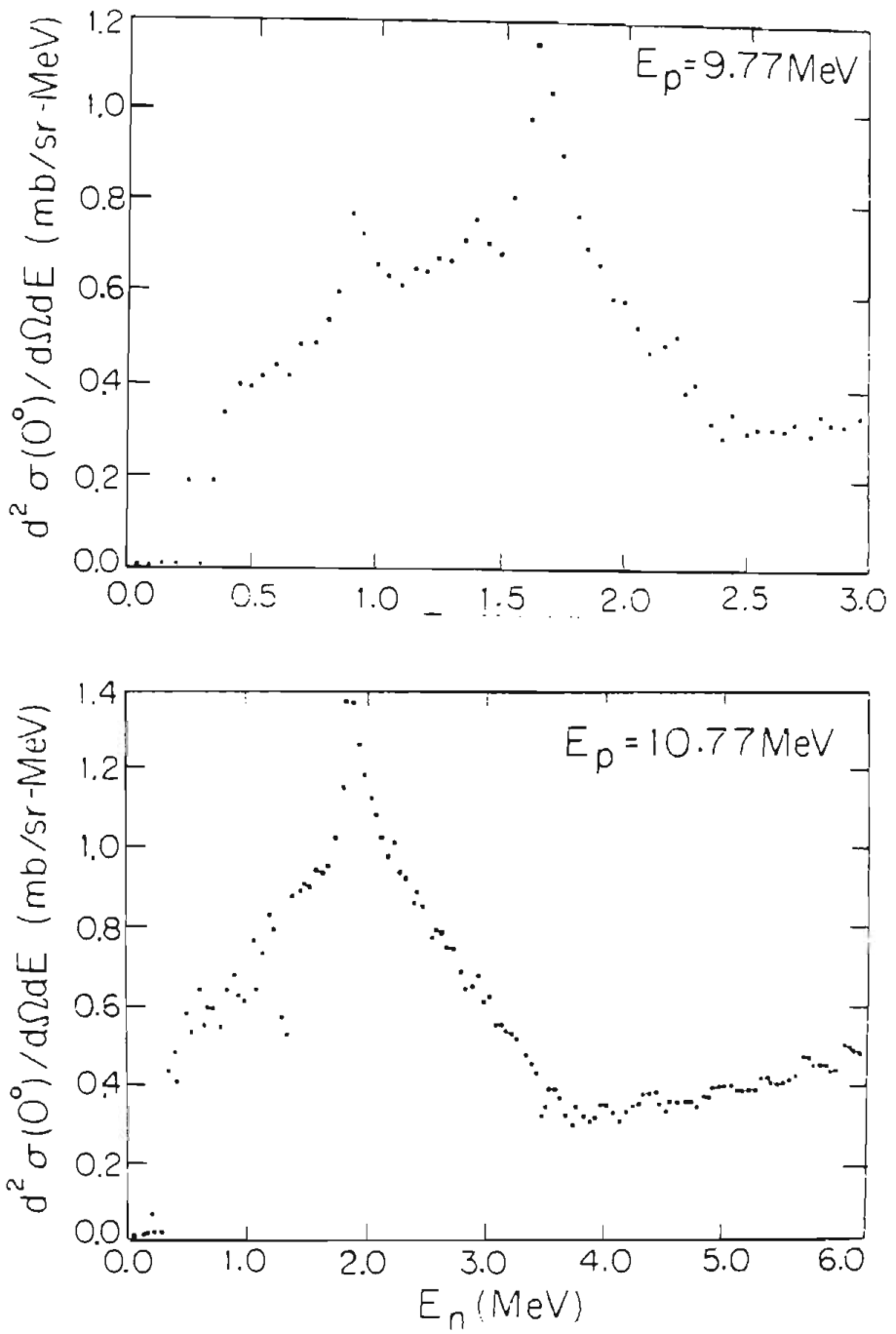

Figure 2.5 Zero-degree double differential cross-sections. (no background has been subtracted).

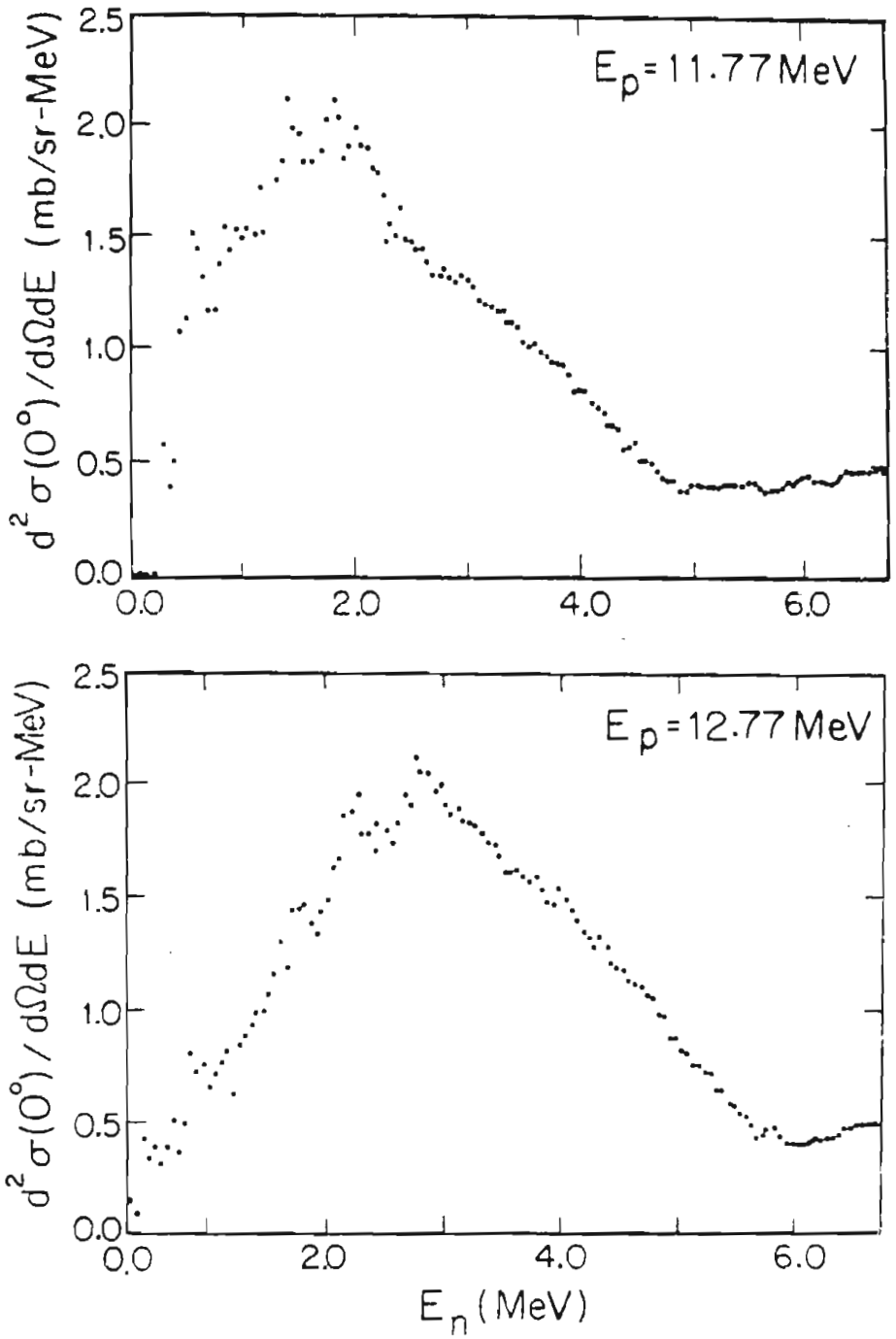

Figure 2.6 Zero-degree double differential cross-sections. (no background has been subtracted).

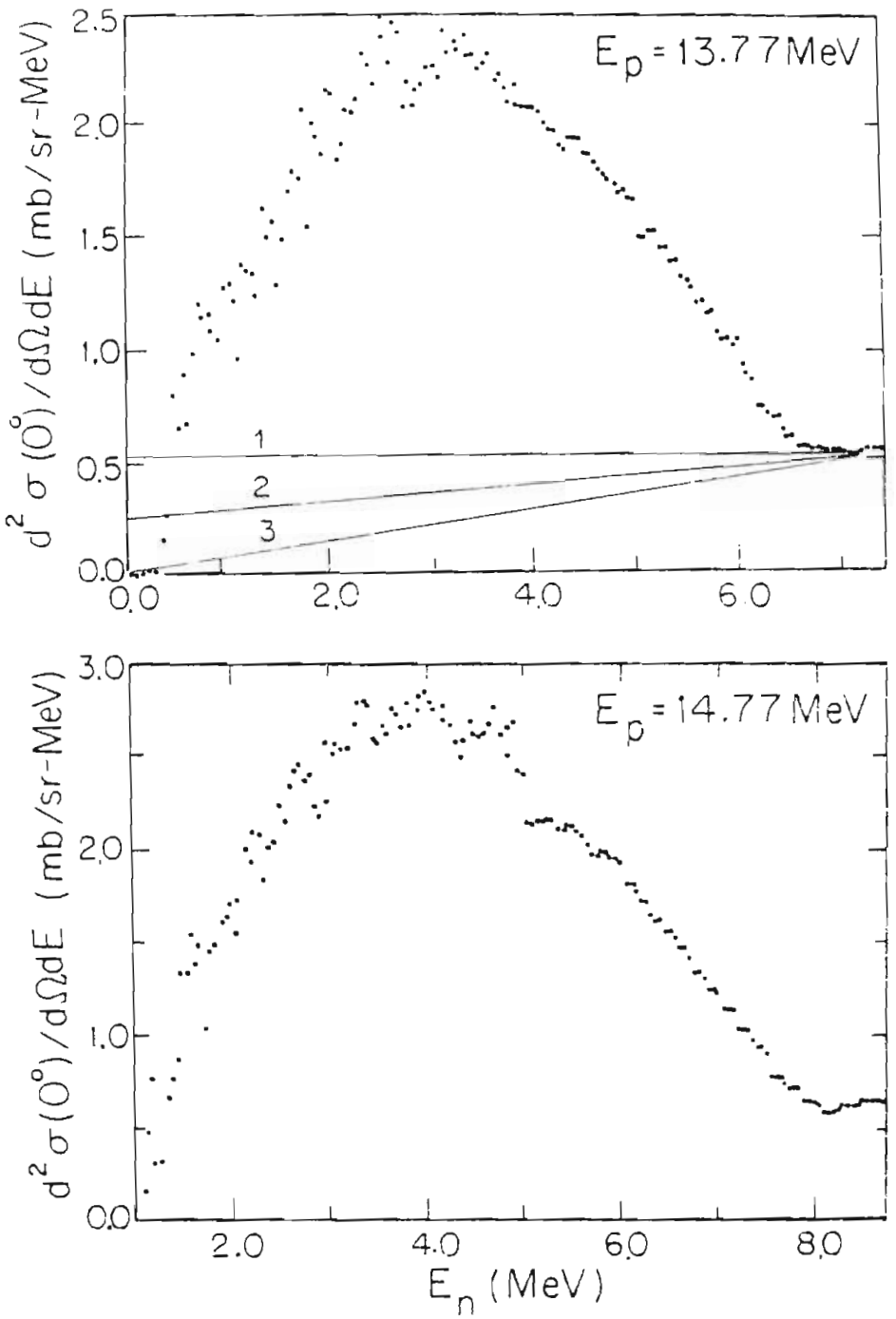

Figure 2.7 Zero-degree double differential cross-sections. In the top figure the straight lines correspond to the three types of backgrounds discussed.

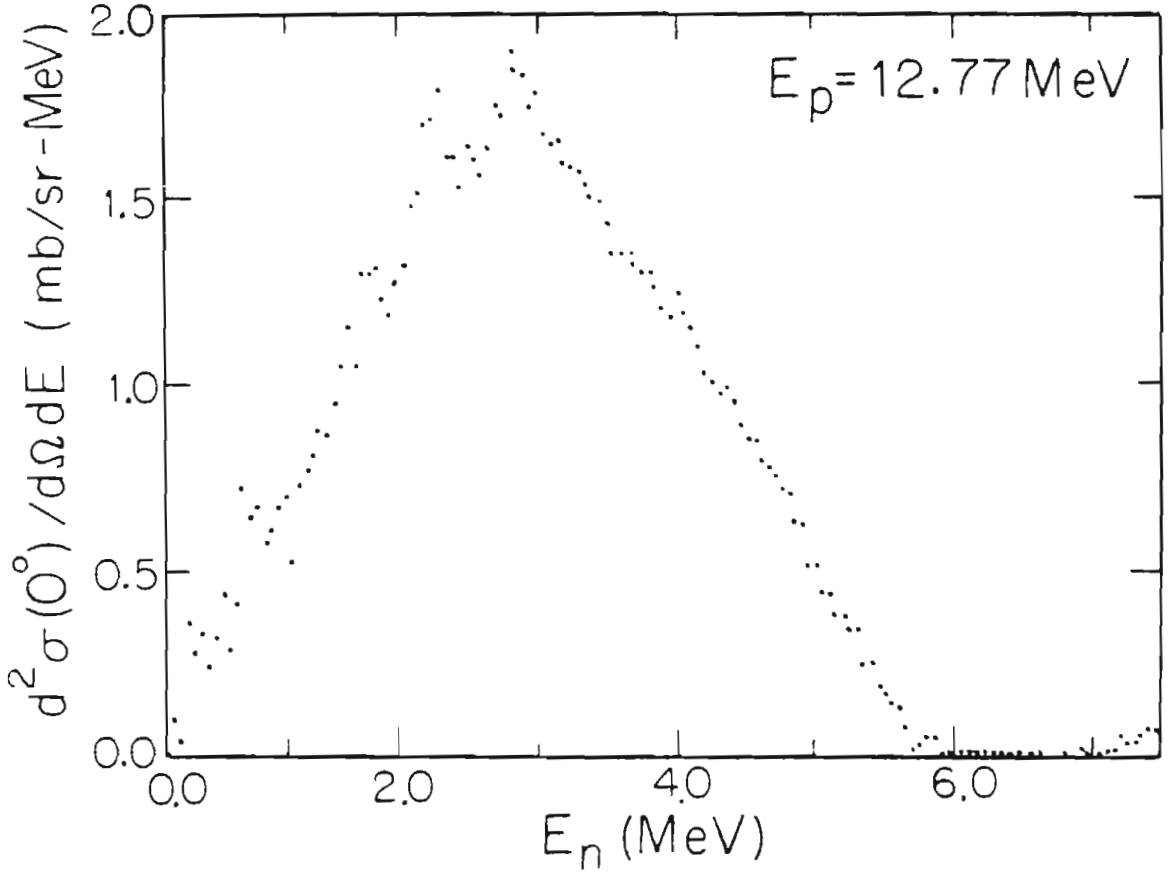

Figure 2.8 Data after subtracting background of type 2 (see fig. 2.7).

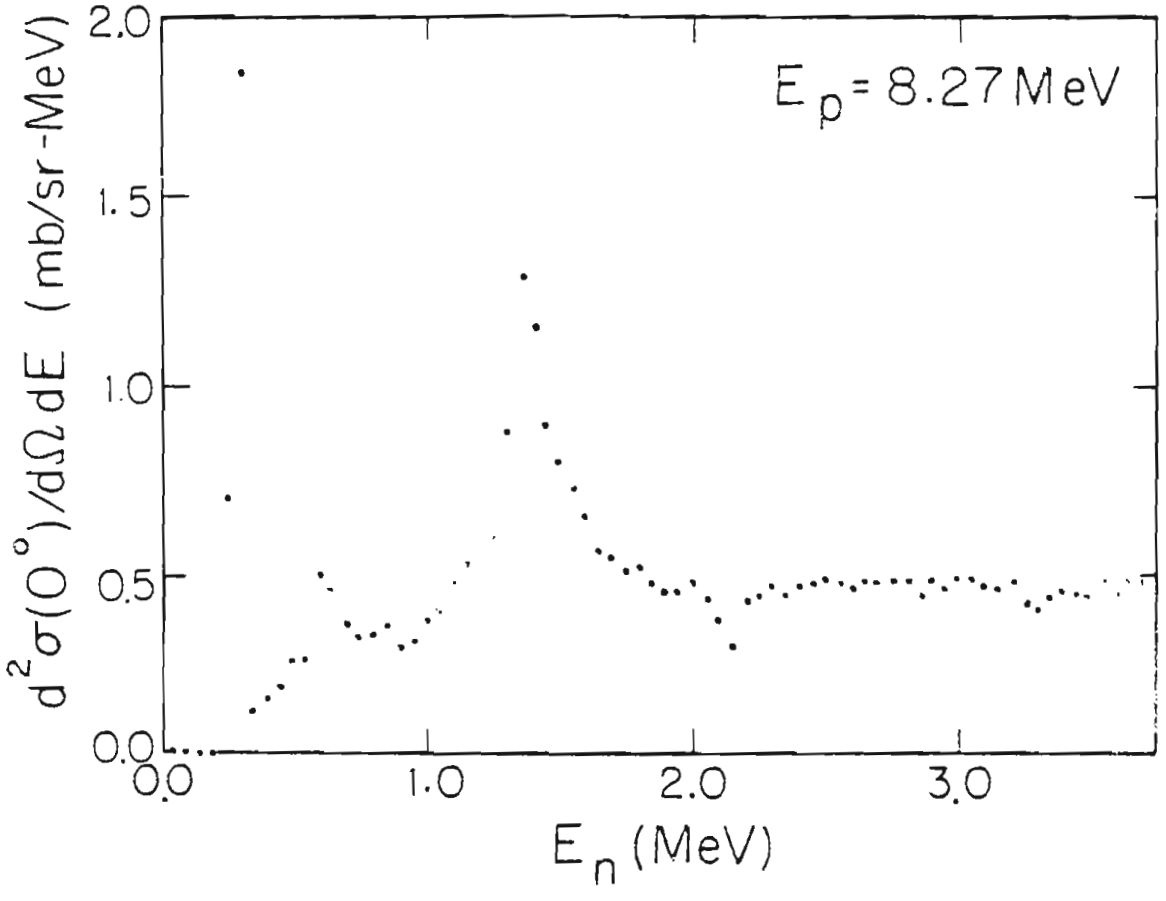

Figure 2.9 Data below threshold for the production of break-up neutrons.

DISCUSSION

Figure 2.10 shows the absolute zero-degree differential cross-sections for neutrons produced by the p+T break-up reactions. The arrows mark the thresholds for three and four body break-up respectively. The data have been subtracted for a background of type 2; these are the final data including errors, all of which are tabulated in table A-1 in the appendix. Included in the same figure are the data of ref.2. There is agreement within error-bars. Our data increase more linearly than the data of ref.2. Appendix A also lists all the zero-degree double-differential cross-sections obtained in the present experiment, including the errors.

The data at 9.77 MeV (fig.2.5) show two very sharp peaks in the break-up region. These cannot be due to break-up into three or four bodies in the final state, because the data at 8.27 MeV which is below threshold (fig.2.9) for these processes also show the peaks. In the 8.27 MeV data the peaks are very prominent and are superimposed on the tail of the primary neutron peak. At 9.77 MeV the ratio of the area of these peaks to the total area in the break-up region is only 0.036 and at 10.77 MeV it is 0.006. The data at 11.77,12.77,13.77 and 14.77 MeV all exhibit these peaks although not so clearly as at 9.77 MeV; the pure break-ups completely overshadow these peaks. Consequently the effect

of these peaks on the total break-up cross-section is insignificant. The two distinct peaks seen at 8.27 MeV seem to increase linearly with increasing proton energy.(There is some doubt as to whether we are identifying the same two peaks at the higher energies, because of the increased structure). At present we believe these peaks are from interactions of the primary neutron flux with the material around the detector and in the shield, and are not associated with tritium break-up.

Data at 14.77 MeV are available only for neutron energies greater than 1.1 MeV. A simple correction was made to account for the cross-section below 1.1 MeV. A half-ellipse resembling the shape of the data was drawn and the ratio of the area in the range 0-1.1 MeV to the area in the range $0\text{-}E_n(max)$ was found. Then the data were corrected accordingly. This correction was made for the data at other energies also, because the bias was set at 0.3 MeV. The corrected and uncorrected cross-sections are tabulated in appendix A.

All the double differential cross-sections obtained in the present experiment are shown in figure 2.11 ;these correspond to a background of type 2. The arrows depict the maximum energy that the neutron can possess at zero-degrees if it resulted from break-up of the type p+T ---> n+d+p. Generally the data is much smoother than that of ref.2.

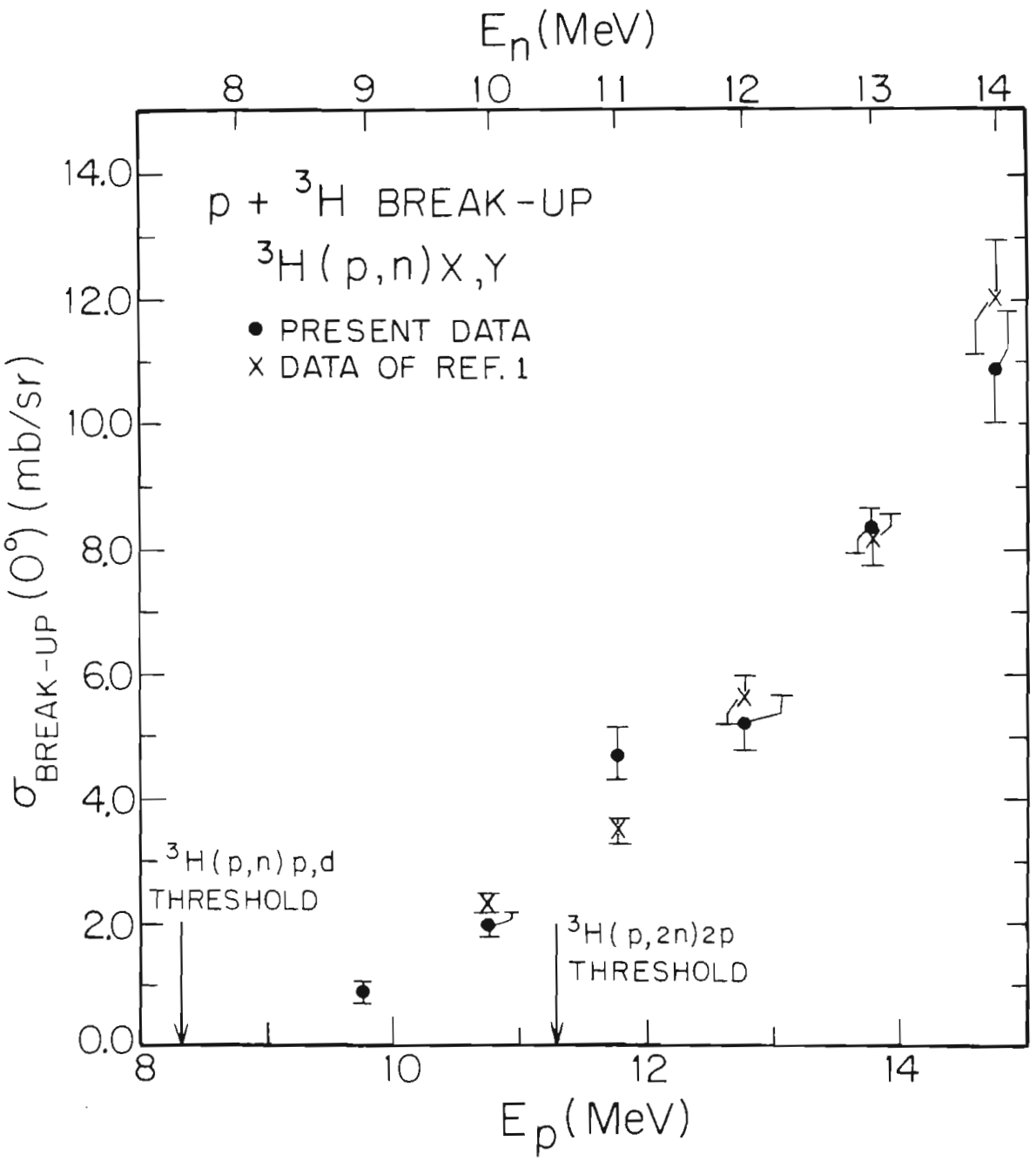

Figure 2.10 Absolute zero-degree differential cross-sections.

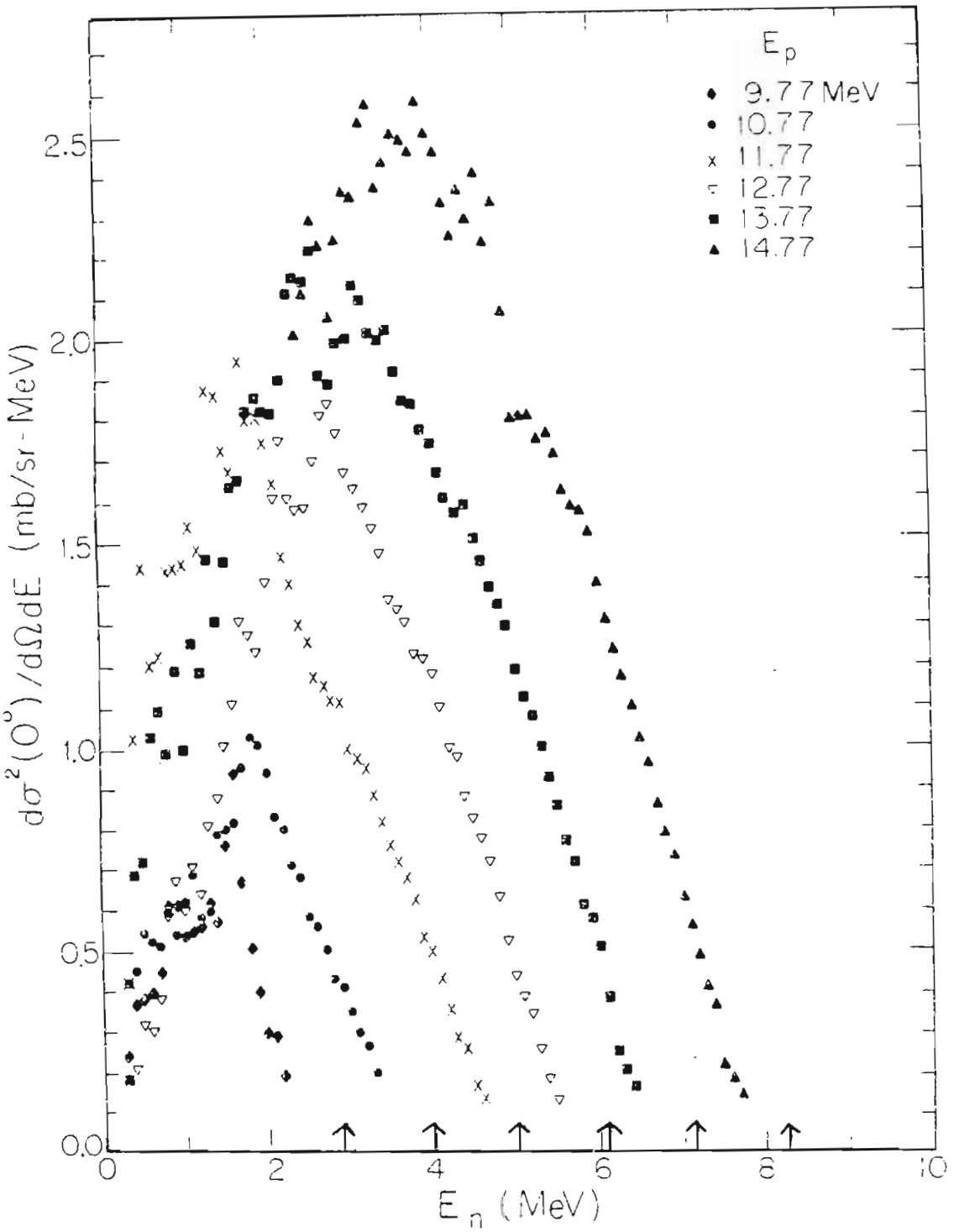

Figure 2.11 Zero-degree double differential cross-sections. (these are the data after background subtraction).

There is some overlap between the 11 and 12 MeV data; in particular, cross-sections at 11 MeV are higher than what we would expect from the trend. This is where we differ most with the data of ref.2. The 'quenching' of the cross-section before reaching threshold (figure 2.11) is as expected because the deuteron and the proton cannot both travel together in the same direction due to Coulomb repulsion (E_n would be maximum when the proton and the deuteron are emitted in the same direction and opposite to that of the neutron).

It is possible to obtain a check on the absolute normalization of the data, based on the yield in the ^{3}He peak, where the cross-section is known accurately. This yield can be predicted knowing the number of target particles, number of incident particles, deadtime, efficiency, solid angle and the cross-section of the $^3H(p,n)^3He$ reaction from ref.2. Table 2.4 lists the ratio of the measured and predicted yields. Figure 2.12 is a plot of these ratios as a function of the primary neutron energy. There is a steady decline in this ratio as the incident proton energy is increased. That the purity of the tritium is changing with time is not a plausible explanation because there is a wide variation in the ratio within the same filling (table 2.4). There is no correlation between the order of the filling and this ratio. Also the gas-pressure did not change during these runs. The last column of table

2.4 lists the ratios after including also the background of type 2 as part of the ^{3}He peak. This does not change the trend. We do not think that there is enough evidence to make a correction to the cross-sections based on these ratios. Here the estimation of the quality of the breakup data was based on the quality of the higher energy data; this may not be fully valid. There is no evidence that any of the experimental conditions deteriorated with increasing proton energy or with time. It could be possible that the beam-current-integration was not complete as the proton energy was increased and as counting rates became very high.

ERRORS

The errors can be classified into two categories: instrumental uncertainties associated with the beam, detection, electronics, deadtime, efficiency, etc., and errors in the data-reduction and normalization procedures. The data used for the normalization (ref.2), typically had an error of less than 2%. Uncertainty in the type of background was the major source of error. As discussed before, the 'tailing' observed is a definite effect and must be accounted for. This would imply that background type 1 (fig.2.6) is not realistic while background type 3 can be taken as an extreme case. We have chosen type 2 and the

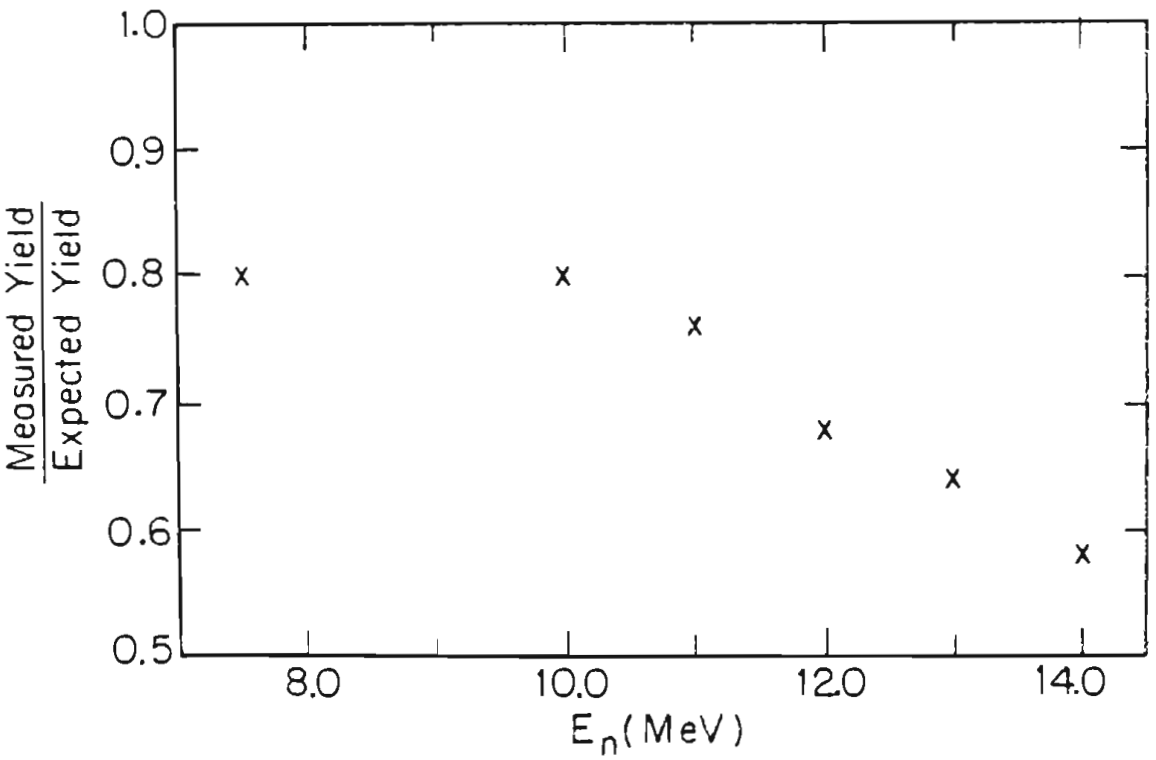

Figure 2.12 Ratios of the measured vs.expected yields in the ground state peak.

uncertainty in this would just be the difference between the backgrounds 2 and 3. Table 2.3 lists the ratio of this difference to the total cross-section (after subtracting type 2 background). Contributions to the errors from other sources are generally much less. These contributions are added in quadrature to that resulting from the uncertainty in the background (type 2 minus type 3). The errors reported in appendix A are from all sources. A flow chart of how the errors were propagated is shown in appendix A.

III

PHASE SPACE

If one knows the momentum $\vec{p}$ and the position $\vec{x}$ of a particle, then its motion is completely determined. The space consisting of the sets $(\vec{x}, \vec{p})$ is known as phase space, where each point in this six-dimensional space corresponds to a definite motion of the particle. In classical mechanics it is possible to make measurements of x, p_x to any desired accuracy. The uncertainty principle limits this by requiring that $\Delta x \Delta p_x \geq 2\pi\hbar$, so that each point in phase space can be known to only $(2\pi\hbar)^3$. This is therefore taken as the volume of the elementary cell in phase-space, for a single particle.

Consider the nuclear reaction A+a ----> b+B+Q where B is assumed to be a sharp and stable state, and we detect particle b only. Then what we observe is σ_B vs. E_b . This cross-section is given by

$$\sigma_B = \frac{2\pi}{\hbar^2} \left| \langle b+B | H | a+A \rangle \right|^2 . \qquad 3\cdot1$$

where H is the interaction Hamiltonian, (b+B) is the final state wave function, and (a+A) the initial state wave function. The spectrum which describes the sharp final

state is entirely described by H . Suppose that the final state is not such a state, but what is observed is a broad distribution corresponding to several final states. Then this information can be included in the formula for the cross-section by the introduction of a factor $\rho(E_b)$ so that

$$\sigma_B = \frac{2\pi}{\hbar^2} |\langle b+B | H | a+A \rangle|^2 \rho(E_b), \qquad 3\text{-}2$$

where $\rho(E_b)$ is called the density of final states or the 'phase space factor'. Now if H is a slowly varying function of energy, then we may approximate the observed spectrum by

$$\sigma_B \propto \rho(E_b) .$$

The factor H assumes a knowledge of the nuclear potential, which is not known exactly. For constant H, the physics of the problem is determined by just the density of states factor. This factor is independent of the interaction potential and is influenced only by the kinematics of the problem. This is relevant to the present experiment because the observed breakup cross-sections follow just such a distribution i.e.

$$\sigma_{\text{break-up}} \propto \text{Number of final States available.}$$

DERIVATION OF THE PHASE SPACE FACTOR[5]

The density of final states can be determined by imposing momentum and energy conservation on the system. Let N be the number of final states available in phase space.

$$\text{Then } N = \frac{\text{Total phase space volume}}{\text{Volume of elementary cell in phase space}}$$

$$= \frac{\int d^3\vec{p} \int d^3\vec{x}}{(2\pi\hbar)^3} \qquad 3\text{-}3$$

The phase space factor $\rho(E)$ is just $\frac{dN}{dE}$. In general, if there are n particles in the final state, then the total number of states available to all the particles, N_n, is given by the product of final states available to each particle.

$$N_n = \frac{\prod_{i=1}^{n} \int d^3\vec{x}_i \int d^3\vec{p}_i}{\left((2\pi\hbar)^3\right)^n} \qquad 3\text{-}4$$

where the integration extends over all possible values of $\vec{x}_i$.

and $\vec{p}_i$. If all the particles are contained in the same geometrical volume, then

$$\int d^3\vec{x}_i = V = \text{constant}$$

so that

$$\frac{dN_n}{dE} = \frac{d}{dE} \int \prod_{i=1}^{n} d^3\vec{p}_i \qquad 3.5$$

(the constant factor will be omitted in all following expressions). In the center-of-mass system $\sum_{i=1}^{n} \vec{p}_i = 0$, which also shows that not all momenta are truly independent; we need to perform the integration over (n-1) particles only. Momentum conservation can be explicitly included in equation 3.5 by using the Dirac delta function. This is done by requiring that

$$\int d^3\vec{p}_n \; \delta^3\left(\vec{p}_n + \sum_{i=1}^{n-1} \vec{p}_i\right) = 1 \qquad 3.6$$

$$\Rightarrow N_n = \int \prod_{j=1}^{n-1} d^3\vec{p}_j \qquad 3.7$$

$$= \int \prod_{j=1}^{n} d^3\vec{p}_j \; \delta^3\left(\sum_{i=1}^{n} \vec{p}_i\right) \qquad 3.8$$

From energy conservation,

$$\sum_{i=1}^{n} E_i = E \quad \text{and} \quad \int dE\, \delta\left(\sum_{i=1}^{n} E_i - E\right) = 1 . \qquad 3.9$$

$$\Rightarrow N_n = \int dE \prod_{j=1}^{n} d^3\vec{p}_j\, \delta^3\left(\sum_{i=1}^{n} \vec{p}_i\right) \delta\left(\sum_{i=1}^{n} E_i - E\right) \qquad 3.10$$

and $$\rho_n(E) = \frac{dN_n}{dE}$$

$$= \int \prod_{j=1}^{n} d^3\vec{p}_j\, \delta^3\left(\sum_{i=1}^{n} \vec{p}_i\right) \delta\left(\sum_{i=1}^{n} E_i - E\right) . \qquad 3.11$$

The differential momentum spectrum of any one of the particles is just $\frac{d\rho_n}{dp_i}$. Several methods are available to evaluate the integrals analytically;[6,7] if there are more than three particles the integrals are non-trivial and numerical codes are available. The method to be used depends on what kinematic quantities are known. If we have information only about the final state, and also the total energy available to the final particles, then one has to evaluate the integrals in equation 3.11 . For three final particles, this expression can be reduced to elliptic integrals of the first, second, and third kinds. The form

of equation 3.11 is not useful if the kinematics of the initial state are well known. A derivation of the density of final states in terms of the Q-value and the incident and detected particle momenta can be obtained quite simply, for three bodies. If only one final particle is detected, then the problem is reduced to essentially a 2-body kinematic calculation because all the other particles can be considered to be a single entity; in this case one just needs to pick an appropriate center-of-mass coordinate system and transform the coordinates into known quantities. The density of states for three final particles when only one of the particles is detected is given by[8]

$$\rho_1\left(E_1^l\right) = \frac{2}{h^6} M^{\frac{1}{2}} \left(m_1 m_2 m_3\right)^{\frac{3}{2}} \times \left(E_1^l \left(\frac{m_2+m_3}{M} E_{tot}^c - E_1^l + 2a_1 \times \left(E_1^l\right)^{\frac{1}{2}} \cos\theta_1^l - a_1^2\right)\right)^{\frac{1}{2}} . \qquad 3.12$$

where m_1, m_2, m_3 are the masses of the 3 final particles

$M = m_1 + m_2 + m_3$; m_p = projectile mass.

m_t = target mass ; $E_{tot}^c = Q + E_p^l/(m_p + m_t)$.

Q = Q-value of reaction

E_p^l = lab. energy of projectile

E_1^l = lab. energy of particle 1 (detected particle).

$a_1 = \left(m_t m_p E_p^l\right)^{\frac{1}{2}} / (m_p + m_t)$

θ_1^l = lab. angle of particle 1.

Using this formula, fits were made to all the break-up data. These fits (figures 3.1 - 3.3) are not particularly good in reproducing the shape of the continuum. The only parameter that was varied in the fitting procedure was the magnitude of the fitting function. The presence of the distinct peaks on top of the continuum may be a reason for the difference in that region; at higher energies, Coulomb repulsion between the deuteron and the proton may explain why the data decreases very much faster. The phase space available to the final particles is the same whether the break-up is direct or whether the break-up occurs in several stages (sequential break-up). A fitting function which includes the 4-body phase space factor and also a term for final state interactions may reproduce the data more accurately.

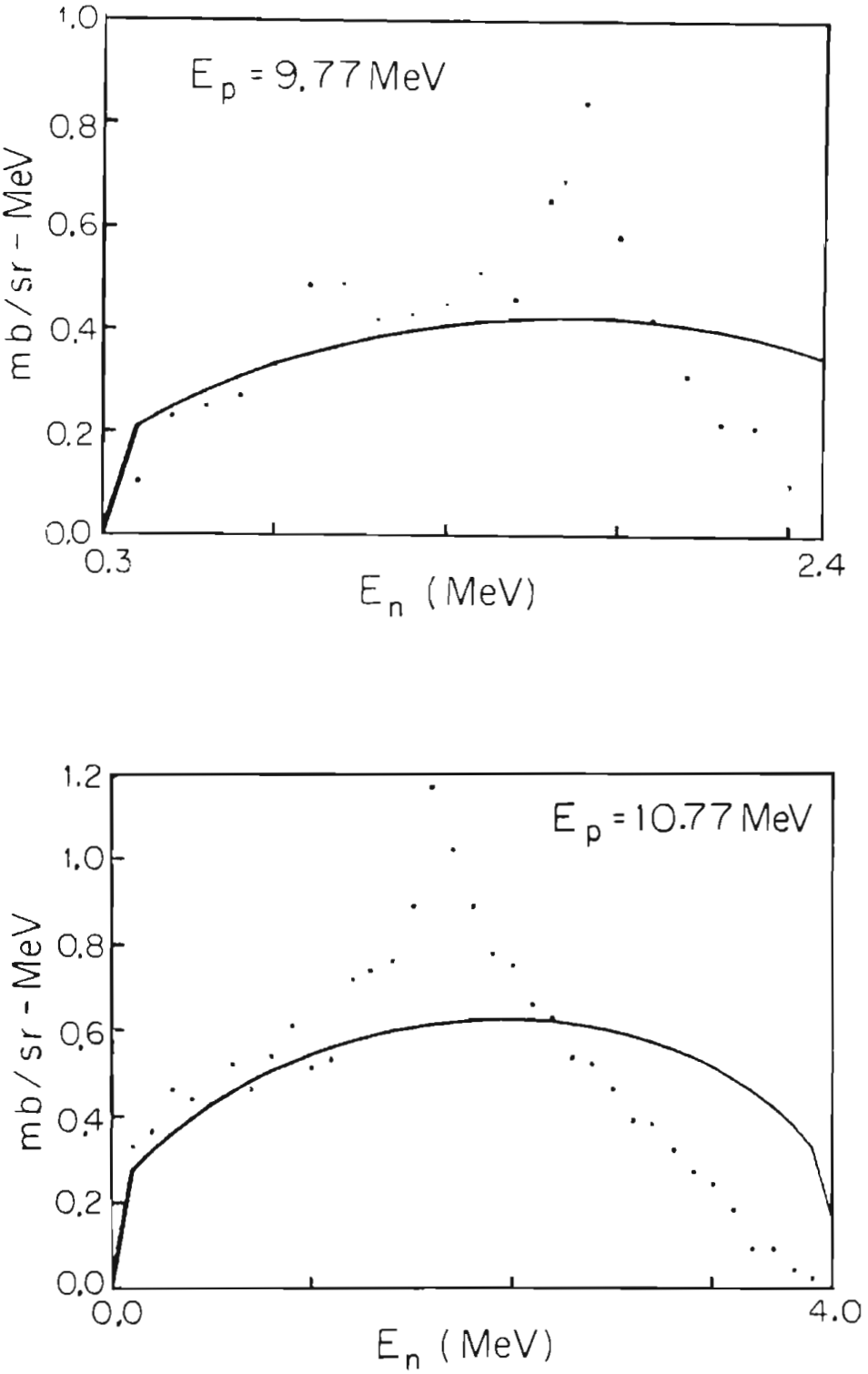

Figure 3.1 Phase-space fits.

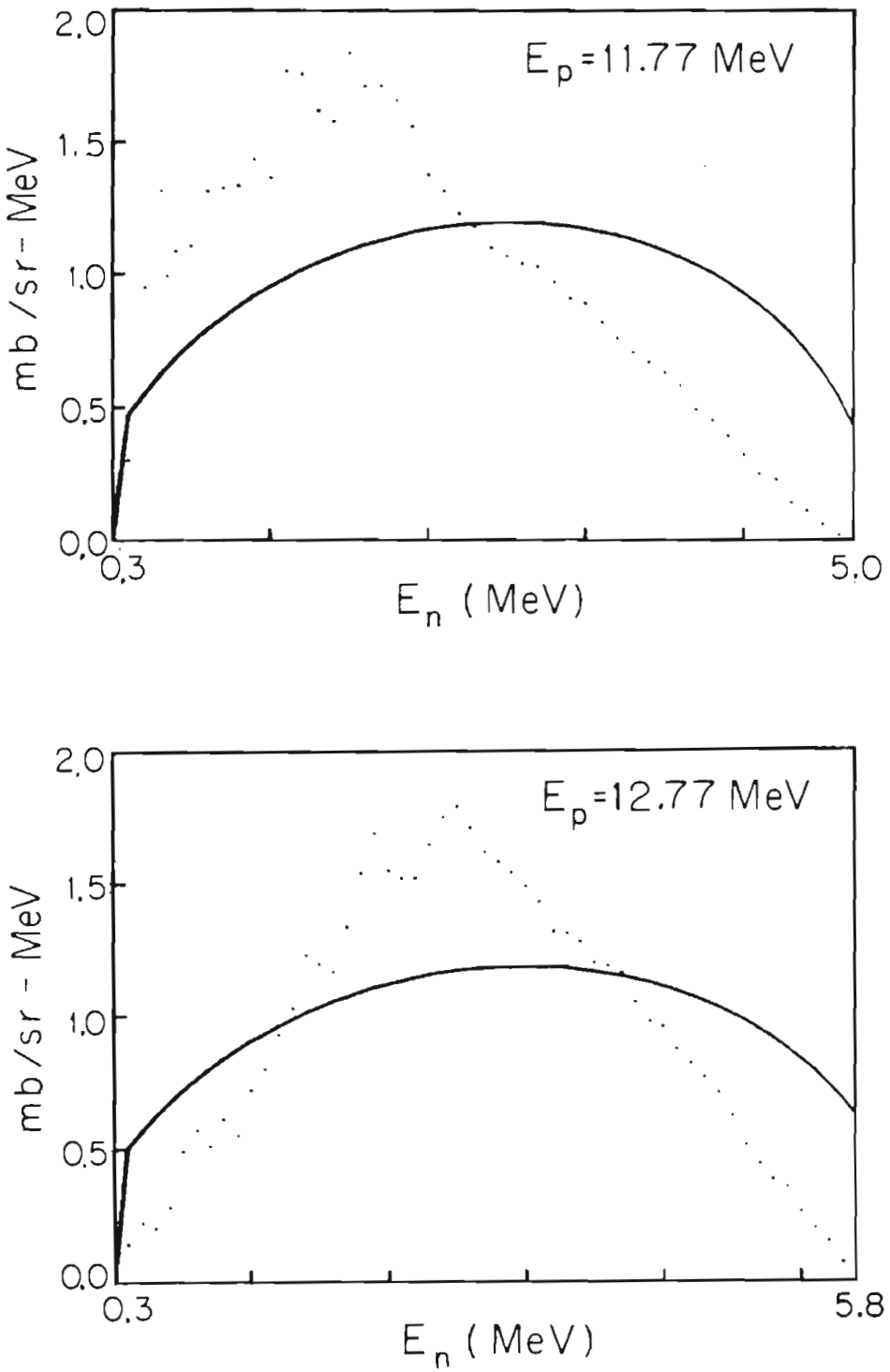

Figure 3.2 Phase-space fits.

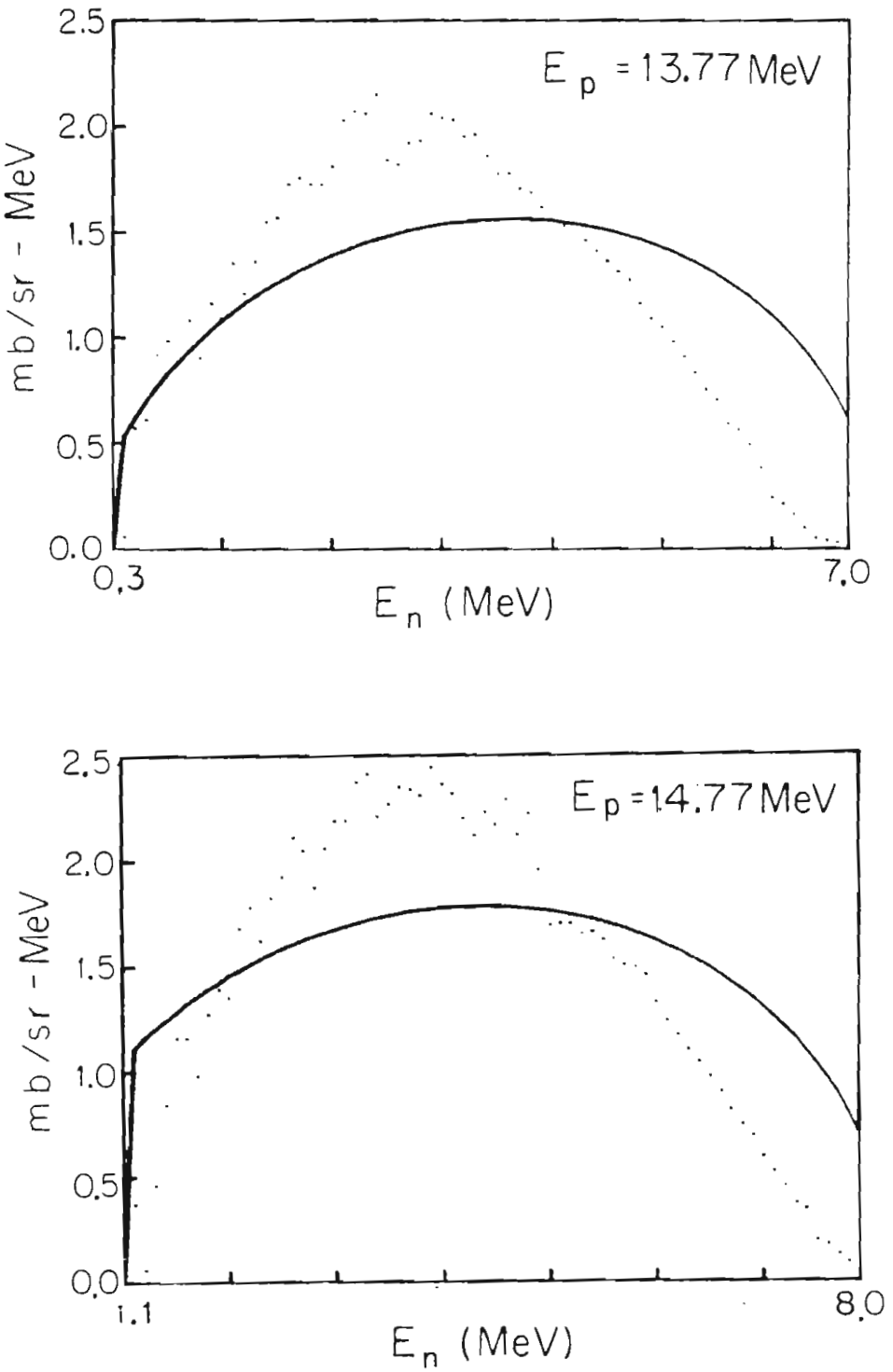

Figure 3.3 Phase-space fits.

SUMMARY

The energy spectra of neutrons produced at zero degrees in the $^{3}H(p,n)$ reactions have been measured for proton energies ranging from 9.77 MeV to 14.77 MeV. Double differential cross sections have been reported and are in reasonable agreement with a previous measurement.[2] A smooth distribution is expected if direct 3-body break-up (n+d+p) is the dominant reaction. However, the theoretical fits to the data are not satisfactory. The differences may indicate the presence of other processes. It would be useful to perform a kinematically complete experiment where more than one of the final particles are detected.

LIST OF REFERENCES

1. Horst Liskien, Arno Paulsen,
Nucl. Data Tables, 11(1973)569, No.7

2. M.Drosg, G.F.Auchampaugh, F.Gurule,
LASL report LA-6459-MS(1976)

3. M.Drosg,
Nucl.Sc.Engg. 67(1978)190.

4. L.W.Seagondollar, P.M.Thambidurai,
Nucl.Instr.Meth. 173(1980)603

5. 'Kinematics and Multiparticle systems', ed.M.Nikolic,
Gordon and Breach Science Publishers, New York.

6. M.M.Block,
Phys.Rev. 101(1956)5,vol.2.

7. T.H.Berlin, George E.Owen,
Nucl.Phys. 5(1958)669.

8. G.G.Ohlsen,
Nucl.Instr.Meth. 37(1965)240.

9. F.O.Purser, Triangle Universities Nuclear Laboratory,
Durham, N.C.

10. F.O.Purser, Triangle Universities Nuclear Laboratory,
Durham, N.C.

11. L.W.Seagondollar, Triangle Universities Nuclear
Laboratory, Durham, N.C.

12. Sadiq El Kadi, Triangle Universities Nuclear Laboratory, Durham, N.C.

13. Albert G.Beyerle, Ph.D. thesis, 1981, North Carolina State University, Raleigh, N.C.

APPENDIX A

Table A-1

Absolute zero-degree differential cross-sections for $^{3}H(p,n)X,Y$.

E_p (MeV)	$\frac{d^2\sigma}{d\Omega\, dE}$ mb/sr *	$\frac{d^2\sigma}{d\Omega\, dE}$ mb/sr **	$\frac{d^2\sigma}{d\Omega\, dE}$ mb/sr ref.2
9.77	0.799 +0.18	0.914 +0.18	
10.77	1.78 +0.24	1.99 +0.24	2.3 +0.1
11.77	4.56 +0.45	4.67 +0.45	3.5 +0.2
12.77	5.11 +0.44	5.20 +0.44	5.6 +0.4
13.77	8.21 +0.42	8.34 +0.42	8.2 +0.4
14.77	9.99 +0.86	10.87 +0.86	12.0 +0.9

* the data in this column have not been corrected for the cross-sections below the bias. This bias was 0.3 MeV for all except the 14.77 MeV data, where the bias was 1.1 MeV.

** This column lists the data which have been corrected for bias.These are the final data. The last column lists the data of ref.2. Figure A-1 describes the errors.

Table A-2

Zero-degree double differential cross-sections
for neutron production by H(p,n)X,Y.
The errors are statistical.

Proton energy = 9.77 MeV

E-neutron MeV	Cross section mb/sr/MeV	Error mb/sr/MeV
0.30	0.10	0.01
0.40	0.23	0.01
0.50	0.25	0.01
0.60	0.27	0.01
0.70	0.33	0.01
0.80	0.49	0.01
0.90	0.49	0.01
1.00	0.42	0.01
1.10	0.43	0.01
1.20	0.45	0.01
1.30	0.51	0.01
1.40	0.46	0.01
1.50	0.65	0.01
1.60	0.84	0.01
1.70	0.58	0.01
1.80	0.42	0.01
1.90	0.31	0.01
2.00	0.22	0.01
2.10	0.21	0.01
2.20	0.10	0.01
2.30	0.01	0.01
2.40	0.02	0.01
2.50	0.00	0.01
2.60	0.00	0.01
2.70	0.00	0.01
2.80	0.00	0.01

Table A-2 (continued)

Proton energy = 10.77 MeV

E-neutron MeV	Cross section mb/sr/MeV	Error mb/sr/MeV
0.30	0.33	0.04
0.40	0.36	0.05
0.50	0.46	0.05
0.60	0.44	0.04
0.70	0.43	0.04
0.80	0.52	0.04
0.90	0.46	0.04
1.00	0.54	0.04
1.10	0.61	0.03
1.20	0.51	0.03
1.30	0.53	0.03
1.40	0.72	0.02
1.50	0.74	0.02
1.60	0.76	0.02
1.70	0.89	0.02
1.80	1.17	0.02
1.90	1.02	0.02
2.00	0.89	0.02
2.10	0.78	0.02
2.20	0.75	0.02
2.30	0.66	0.02
2.40	0.63	0.02
2.50	0.54	0.02
2.60	0.52	0.02
2.70	0.46	0.02
2.80	0.39	0.02
2.90	0.38	0.02
3.00	0.32	0.02
3.10	0.27	0.02
3.20	0.24	0.02
3.30	0.18	0.02
3.40	0.09	0.02
3.50	0.09	0.02
3.60	0.04	0.02
3.70	0.02	0.02
3.80	0.00	0.02
3.90	0.01	0.02
4.00	0.01	0.02

Table A-1 (continued)

Proton energy = 11.77 MeV

E-neutron MeV	Cross section mb/sr/MeV	Error mb/sr/MeV
0.30	0.30	0.05
0.40	0.95	0.07
0.50	1.32	0.07
0.60	1.09	0.06
0.70	1.11	0.06
0.80	1.32	0.06
0.90	1.33	0.06
1.00	1.34	0.06
1.10	1.44	0.06
1.20	1.37	0.06
1.30	1.77	0.07
1.40	1.76	0.06
1.50	1.62	0.06
1.60	1.58	0.06
1.70	1.84	0.05
1.80	1.71	0.05
1.90	1.71	0.05
2.00	1.66	0.04
2.10	1.56	0.03
2.20	1.38	0.03
2.30	1.32	0.03
2.40	1.23	0.03
2.50	1.18	0.03
2.60	1.10	0.02
2.70	1.07	0.02
2.80	1.04	0.02
2.90	1.03	0.03
3.00	0.97	0.03
3.10	0.91	0.03
3.20	0.89	0.03
3.30	0.82	0.03
3.40	0.76	0.02
3.50	0.71	0.02
3.60	0.67	0.02
3.70	0.63	0.03
3.80	0.58	0.02
3.90	0.49	0.03
4.00	0.45	0.02
4.10	0.39	0.02

Table A-2 (continued)

Proton energy = 11.77 MeV

E-neutron MeV	Cross section mb/sr/MeV	Error mb/sr/MeV
4.20	0.32	0.03
4.30	0.25	0.02
4.40	0.23	0.02
4.50	0.14	0.02
4.60	0.11	0.02
4.70	0.06	0.03
4.80	0.02	0.03
4.90	0.01	0.02
5.00	0.01	0.02

Table A-2 (continued)

Proton energy = 12.77 MeV

E-neutron MeV	Cross section mb/sr/MeV	Error mb/sr/MeV
0.30	0.00	0.06
0.40	0.14	0.08
0.50	0.22	0.08
0.60	0.20	0.07
0.70	0.28	0.08
0.80	0.49	0.08
0.90	0.57	0.08
1.00	0.51	0.08
1.10	0.61	0.08
1.20	0.55	0.09
1.30	0.72	0.09
1.40	0.80	0.07
1.50	0.93	0.07
1.60	1.03	0.08
1.70	1.23	0.07
1.80	1.20	0.06
1.90	1.17	0.06
2.00	1.34	0.06
2.10	1.54	0.06
2.20	1.69	0.05
2.30	1.55	0.06
2.40	1.52	0.05
2.50	1.52	0.06
2.60	1.65	0.05
2.70	1.75	0.05
2.80	1.79	0.05
2.90	1.71	0.03
3.00	1.62	0.03
3.10	1.58	0.03
3.20	1.54	0.03
3.30	1.49	0.02
3.40	1.43	0.02
3.50	1.32	0.03
3.60	1.31	0.03
3.70	1.28	0.03
3.80	1.20	0.03
3.90	1.19	0.03
4.00	1.16	0.03
4.10	1.05	0.03
4.20	0.98	0.03
4.30	0.96	0.03
4.40	0.87	0.03

Table A-2 (continued)

Proton energy = 12.77 MeV

E-neutron MeV	Cross section mb/sr/MeV	Error mb/sr/MeV
4.50	0.82	0.03
4.60	0.77	0.03
4.70	0.71	0.03
4.80	0.62	0.03
4.90	0.51	0.03
5.00	0.44	0.03
5.10	0.38	0.03
5.20	0.35	0.02
5.30	0.26	0.03
5.40	0.20	0.03
5.50	0.15	0.03
5.60	0.07	0.03
5.70	0.06	0.02
5.80	0.05	0.03
5.90	0.00	0.03
6.00	0.00	0.03
6.10	0.00	0.03

Table A-2 (continued)

Proton energy = 13.77 MeV

E-neutron MeV	Cross section mb/sr/MeV	Error mb/sr/MeV
0.30	0.06	0.07
0.40	0.57	0.10
0.50	0.61	0.10
0.60	0.91	0.10
0.70	0.98	0.10
0.80	0.88	0.10
0.90	1.08	0.10
1.00	0.90	0.10
1.10	1.16	0.10
1.20	1.09	0.09
1.30	1.35	0.10
1.40	1.21	0.09
1.50	1.36	0.10
1.60	1.55	0.09
1.70	1.57	0.10
1.80	1.73	0.09
1.90	1.76	0.09
2.00	1.73	0.09
2.10	1.73	0.08
2.20	1.81	0.08
2.30	2.03	0.08
2.40	2.07	0.08
2.50	2.06	0.08
2.60	2.15	0.06
2.70	1.84	0.06
2.80	1.82	0.06
2.90	1.92	0.06
3.00	1.93	0.07
3.10	2.06	0.07
3.20	2.04	0.07
3.30	2.03	0.07
3.40	1.95	0.06
3.50	1.96	0.04
3.60	1.86	0.05
3.70	1.78	0.05
3.80	1.78	0.05
3.90	1.71	0.05
4.00	1.69	0.04
4.10	1.62	0.03
4.20	1.56	0.04
4.30	1.53	0.03
4.40	1.54	0.04

Table A-2 (continued)

Proton energy = 13.77 MeV

E-neutron MeV	Cross section mb/sr/MeV	Error mb/sr/MeV
4.50	1.46	0.03
4.60	1.41	0.04
4.70	1.36	0.04
4.80	1.31	0.04
4.90	1.27	0.03
5.00	1.16	0.03
5.10	1.09	0.03
5.20	1.05	0.03
5.30	0.98	0.04
5.40	0.91	0.04
5.50	0.83	0.03
5.60	0.75	0.03
5.70	0.70	0.04
5.80	0.59	0.04
5.90	0.56	0.03
6.00	0.49	0.04
6.10	0.38	0.03
6.20	0.24	0.03
6.30	0.21	0.03
6.40	0.16	0.03
6.50	0.10	0.03
6.60	0.05	0.03
6.70	0.04	0.03
6.80	0.03	0.03
6.90	0.02	0.03
7.00	0.01	0.03
7.10	0.00	0.03
7.20	0.00	0.03

Table A-2 (continued)

Proton energy = 14.77 MeV

E-neutron MeV	Cross section mb/sr/MeV	Error mb/sr/MeV
1.10	0.37	0.05
1.20	0.06	0.02
1.30	0.46	0.05
1.40	0.84	0.08
1.50	1.16	0.10
1.60	1.16	0.10
1.70	0.98	0.09
1.80	1.27	0.11
1.90	1.39	0.12
2.00	1.35	0.12
2.10	1.68	0.14
2.20	1.78	0.15
2.30	1.62	0.11
2.40	1.82	0.10
2.50	1.92	0.09
2.60	2.11	0.11
2.70	2.05	0.08
2.80	1.87	0.10
2.90	2.06	0.05
3.00	2.19	0.06
3.10	2.19	0.07
3.20	2.37	0.07
3.30	2.41	0.06
3.40	2.21	0.04
3.50	2.27	0.09
3.60	2.35	0.07
3.70	2.34	0.07
3.80	2.31	0.08
3.90	2.44	0.07
4.00	2.36	0.07
4.10	2.32	0.06
4.20	2.20	0.07
4.30	2.12	0.07
4.40	2.23	0.08
4.50	2.17	0.06
4.60	2.29	0.07
4.70	2.12	0.07
4.80	2.22	0.08
4.90	1.95	0.05

Table A-2 (continued)

Proton energy = 14.77 MeV

E-neutron MeV	Cross section mb/sr/MeV	Error mb/sr/MeV
5.00	1.69	0.05
5.10	1.70	0.04
5.20	1.70	0.05
5.30	1.65	0.05
5.40	1.66	0.04
5.50	1.62	0.04
5.60	1.53	0.03
5.70	1.50	0.03
5.80	1.49	0.03
5.90	1.45	0.03
6.00	1.32	0.04
6.10	1.24	0.03
6.20	1.17	0.03
6.30	1.10	0.03
6.40	1.04	0.03
6.50	0.97	0.03
6.60	0.90	0.03
6.70	0.81	0.03
6.80	0.74	0.03
6.90	0.69	0.03
7.00	0.59	0.03
7.10	0.52	0.02
7.20	0.45	0.03
7.30	0.37	0.03
7.40	0.34	0.02
7.50	0.19	0.03
7.60	0.17	0.03
7.70	0.13	0.03
7.80	0.09	0.03
7.90	0.04	0.03
8.00	0.02	0.02
8.10	0.00	0.03
8.20	0.00	0.02

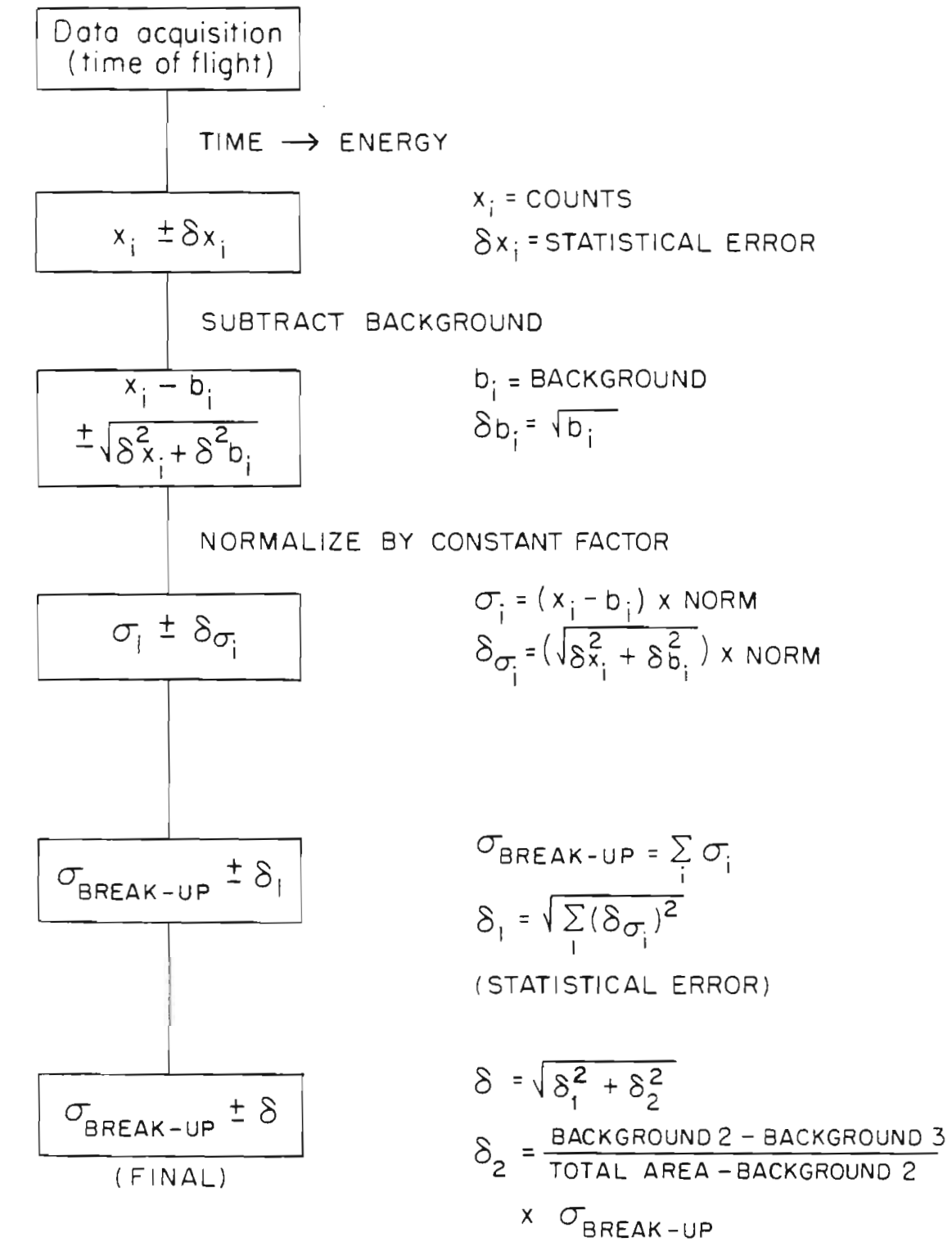

[THE ERRORS IN TABLE A-1 ARE δ;
THOSE IN TABLE A-2 ARE δ_{σ_i}]

Figure A-1 Propagation of errors.